Iron Removal in Low Salinity Water

A case study of brackish water reverse osmosis permeate

Master Thesis

Agung Kusumawardhana

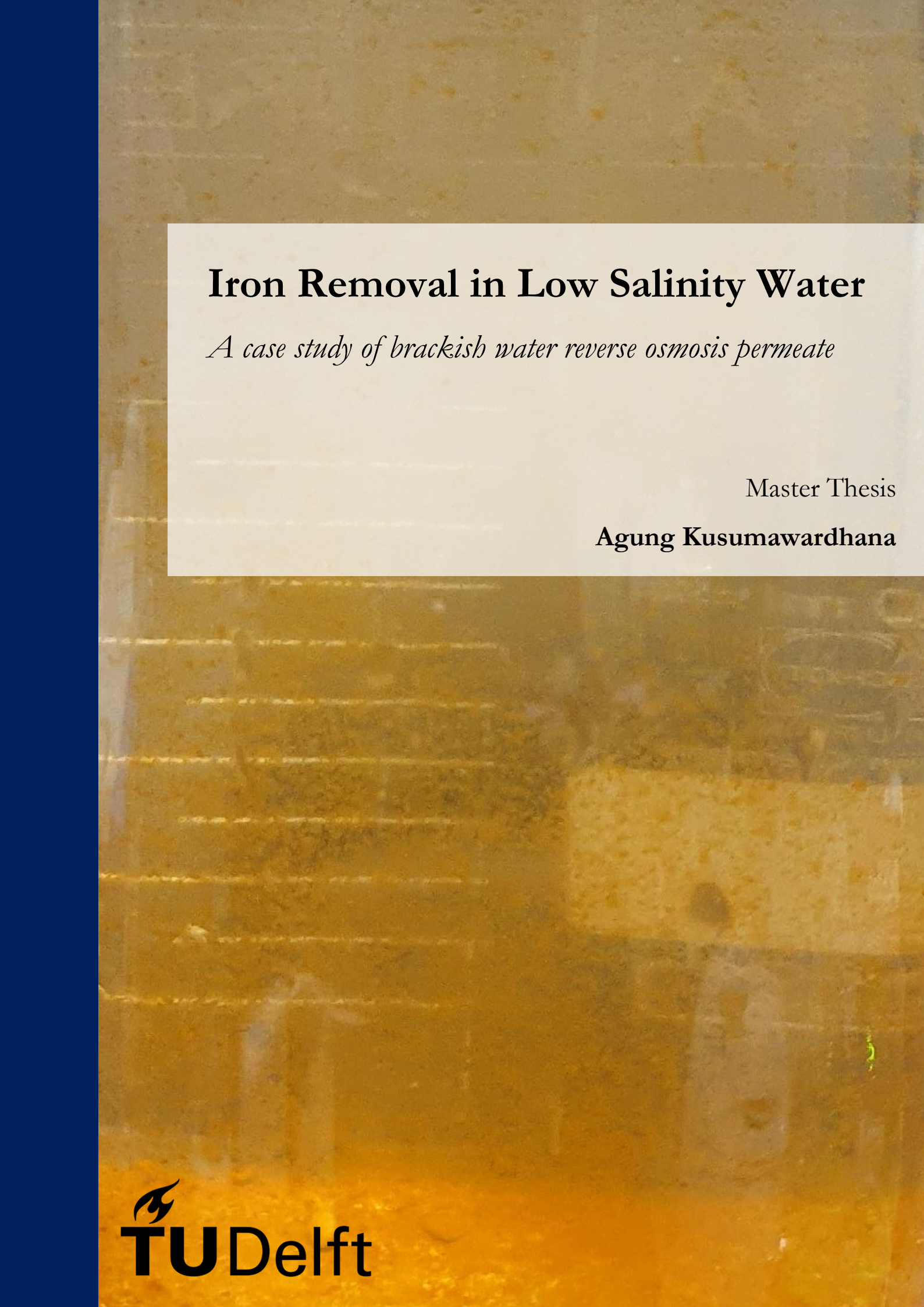

TU Delft

This page is intentionally left blank

Iron Removal in Low Salinity Water

A case study of brackish water reverse osmosis permeate

By

Agung Kusumawardhana

In partial fulfilment of the requirements for the degree of

Master of Science
In Civil Engineering

at the Delft University of Technology,

To be defended publicly on 27 August 2021

Thesis committee:	Prof. dr. Ir. L. C. Rietveld	TU Delft
	Dr. Ir. S. G. J. Heijman	TU Delft
	Dr. Ir. Henri Spanjers	TU Delft
	Dr. Amir H. Haidari	Hatenboer-Water

TU Delft HATENBOERWATER

This page is intentionally left blank

Acknowledgment

This thesis is the finale of my Master's program at TU Delft as a result of 9 months of laboratory work and desk study. I would like to express my gratitude to my daily supervisors Bas Heijman and Amir Haidari for their supervision while doing my graduation work and guidance that put me back on track when I was lost during my thesis work. I also would like to thank my graduation committee Luuk Rietveld and Henri Spanjers for their valuable feedback on my work. Lastly, I would like to thank my parents that always prayed for my well-being especially during the pandemic. I also would like to thank all my friends in Delft that have supported me and kept me sane during the lockdown period.

This page is intentionally left blank

Abstract

A reverse osmosis (RO) membrane is used by an agricultural company in Emmen to treat brackish groundwater to supply water for growing crops and cleaning purposes. However, the RO membrane has only the ability to remove 95-98% of iron from the groundwater and the permeate contains iron in the range of 1.14 – 1.28 mg/L. To be able to remove the remaining iron from the permeate of RO, rapid sand filters are used. To have efficient removal of iron by rapid sand filters, an aeration tower is installed to remove gases such as methane, H_2S, and CO_2, thereby increasing the pH to <7 after aeration. The treatment units (packed tower aerator and rapid sand filter) can remove the iron most of the time throughout the year. However, the farmer periodically (once per year) reported yellowish treated water, indicating insufficient iron removal. Nevertheless, it is still not clear what is the cause of the insufficiency of the iron removal.

Thus, this thesis aimed to investigate the iron removal in the water treatment plant in Emmen and propose a solution to improve the iron removal. The iron removal of the treatment plant was investigated through a set of batch iron oxidation, flocculation, and filtration experiments. Synthetic permeate was used in the experiments following the components of the real permeate in the treatment plant. The pH, concentration of nitrate, and concentration of bicarbonate were varied. The oxidation of Fe(II) was conducted using jar test apparatus. The iron flocs were filtered through 0.2 µm filters and a sand column filter to investigate the filterability of the flocs. In addition, the adsorption of Fe(II) in the column filter was also investigated. To compare the results with previous studies, modeling of Fe(II) oxidation using Phreeqc and adsorption breakthrough of Fe(II) using COMSOL were conducted.

The pH of the water was the main parameter that influenced the oxidation of Fe(II). It was found through experiment and modeling that within the retention time that was available in the treatment plant's tower aerator and the rapid sand filter (20 minutes), the Fe(II) was not fully oxidized and flocculated. At pH of the permeate in the range of 6 – 7, only <11.5% of the initial Fe(II) was oxidized in 20 minutes. Increasing the pH to 8 accelerated the oxidation of Fe(II), and the Fe(II) was completely oxidized within 30 minutes.

Although removal of iron that is dominated by floc filtration was not achieved, the treatment plant also removed the iron through adsorption on iron hydroxide deposit in the packed tower aerator and sand particle. However, the Fe(II) adsorption capacity of adsorbents was low at low pH. The regeneration of the adsorption capacity was achieved through oxidation of the adsorbed Fe(II) which is also influenced by pH. COMSOL model showed that without regeneration, the adsorption capacity of new sand and iron oxide-coated sand was exhausted after 24 hours and 230 hours, respectively.

When the concentration of CO_2 in the permeate is in equilibrium with air, the pH of the permeate should be in the range of 7.9 – 8. However, the maximum pH of the permeate was 7 after aeration because the contact time of the tower aerator was not sufficient to completely strip the CO_2. The tower aerator was also clogged by iron deposits that reduces the airflow and causes short-circuiting that decrease the CO_2 stripping efficiency over time.

Installation of a bubble column reactor was proposed to improve the CO_2 stripping and increase the pH of the permeate. The Phreeqc model showed that the CO_2 could be stripped until approx. 1 mg/L within 4 minutes, and the pH also increased to approx. 7.9. Moreover, the bubble column reactor will provide additional retention time for Fe(II) oxidation, and approx. 20 – 30% of the initial Fe(II) concentration can be oxidized within 4 minutes. The bubble column was considered preferable compared to the packed tower aerator because it was not susceptible to clogging by iron deposits and requires lower maintenance.

This page is intentionally left blank

Table of Contents

List of Figures

List of Tables

1 Introduction

1.1.Treatment of groundwater for agricultural use (a case in Emmen)

An agricultural company in Emmen uses brackish groundwater to supply water for growing crops and cleaning purposes. The groundwater is directly passed through cartridge filters and a reverse osmosis membrane. Because gases in the water can pass through the reverse osmosis (RO) membrane, the gases are removed using a packed tower aerator. After aeration, the water passes through a sand filter to remove the remaining iron from the permeate of RO, and storage is provided after sand filtration. The process scheme is illustrated in Figures 1.1 and 1.2.

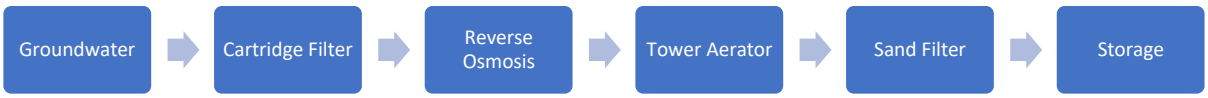

Figure 1. 1 Process scheme of the groundwater treatment plant in Emmen

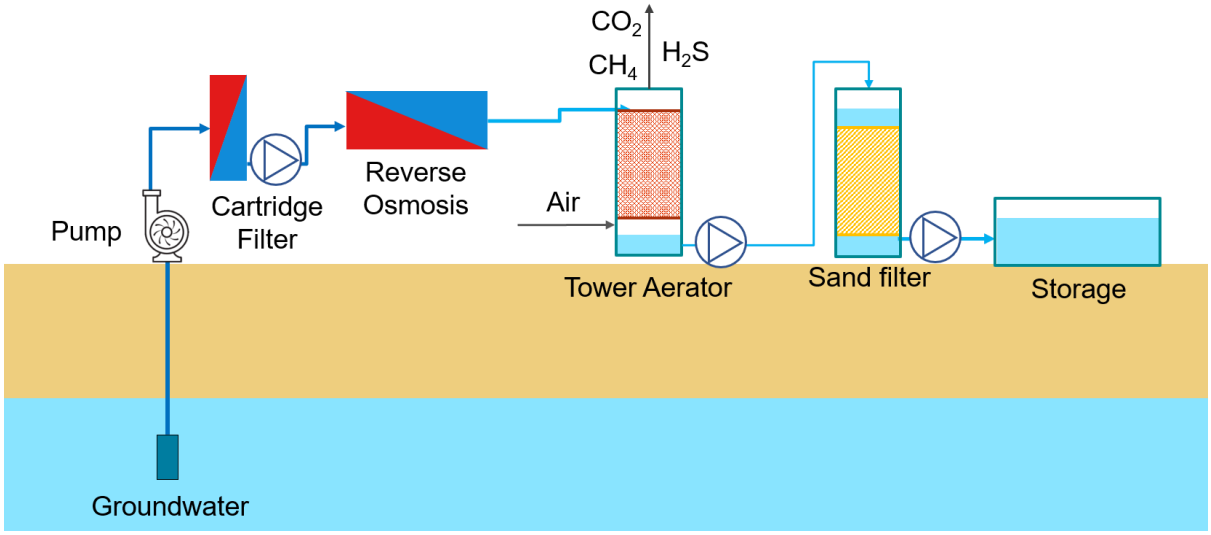

Figure 1. 2 Illustration of the treatment train in the groundwater treatment plant in Emmen

1.2.Problem definition

Most of the time throughout the year, the treatment plant produces water of the desired quality. Nevertheless, sometimes the water that is used for cleaning the glasses of greenhouse can cause orange/yellowish colour, indicating iron content in the water. The farmer reported this problem about once in a couple of years.

Although infrequent, the concentration of iron in the range of 0.15 – 0.22 mg/L already poses a potential hazard to irrigation systems, especially drip irrigation (Netafim, 2012). A more severe problem of clogging can also arise if the concentration of iron is above 1.5 mg/L (Ford, 1994; Netafim, 2012). Aside from clogging of the irrigation system, an iron concentration above 0.3 mg/L can lead to

iron hydroxide stains on leaves and discoloration on foliage plants when overhead irrigation is used (Zinati & Shuai, 2005).

Moreover, the farmer uses the produced water for cleaning purposes and iron can stain glasses of greenhouse and other surfaces. The wet glass surface has a negative charge that attracts positively charged Fe(II) and Fe(III) ions. The oxidation of the Fe(II) on the glass surface and the reaction of Fe(III) with the glass surface lead to the formation of ferric hydrosilicate stain (Marboe & Weyl, 1947).

The concentration of total iron in the feed water to RO varies in the range of 5 – 23 mg/L. After RO, the permeate contains 1.14 – 1.73 mg/L of Fe(II) (Hatenboer-Water, 2020). It was expected that the tower aerator will provide oxygen that can allow the oxidation of Fe(II) into Fe(III) that will subsequently be flocculated and removed by the rapid sand filter. It was also expected that the aeration process will strip CO_2 from the water and increase the pH. However, the pH only increases from the initial pH of 5.7 – 6.2 before aeration to 6.4 – 7 after aeration.

As the oxidation rate of Fe(II) is highly affected by pH (Stumm & Lee, 1961), it is expected that the low pH of the permeate makes the oxidation of Fe(II) slow. The low temperature of the permeate of 12°C – 15°C and the presence of other ions may also contribute to the slow oxidation rate (Sung & Morgan, 1980). In addition, the low initial Fe(II) concentration may also contribute to the slow oxidation rate due to the low catalytic effect from Fe(III) (El Azher et al., 2008).

The water treatment plant in Emmen is located in an agricultural area where fertilizer is widely applied to increase crop production. Although fertilizer input is crucial for agricultural production, extensive use of fertilizer can lead to higher nitrate contamination in groundwater (Wick et al., 2012).

The RO membrane of the water treatment plant has a nitrate rejection efficiency of about 92% (Hatenboer-Water, 2020). Other studies have reported nitrate rejection by RO membrane in the range of 76% – 98% depending on the type of RO membrane that is used (Bohdziewicz et al., 1999; Madaeni & Koocheki, 2010; Molinari et al., 2001; Schoeman & Steyn, 2003). It was observed that the permeate contains nitrate in the range of 6.3 – 12 mg/L.

It was suspected that nitrate hinders the flocculation of iron and reduces the removal of iron floc by the rapid sand filter as phosphate does (Voegelin et al., 2009). Nevertheless, only one study by Tamura et al. (1976) mentions the oxidation of Fe(II) in the presence of nitrate. However, Tamura et al. (1976) did not vary the concentration of nitrate, thus the effect of different nitrate concentrations on Fe(II) oxidation is not yet known. Moreover, although the effect of phosphate on iron flocculation has been widely studied (Kaegi et al., 2010; Voegelin et al., 2009), the effect of nitrate on iron flocculation could not be found in previous literature.

Aside from nitrate, the use of fertilizer in the agricultural area can also release phosphorus into the groundwater (Domagalski & Johnson, 2011). Previous studies have shown that phosphate hinders the flocculation of Fe(III)hydroxides (Kaegi et al., 2010; Mitra & Matthews, 1985; Voegelin et al., 2009). The measurement from the groundwater in Emmen and the permeate resulted in phosphorus concentration that is below the detection limit (Hatenboer-Water, 2020). Therefore, it was expected that the absence of phosphate in the permeate does not hinder the flocculation of Fe(III) hydroxide.

At this point, the cause of the presence of iron in the produced water is still unclear and further investigation is needed to determine the cause of the problem and the solution.

1.3.Research scope

1.3.1. Research objectives and hypothesis

The goal of this research is to investigate the cause of the insufficient iron removal and find a solution to improve the iron removal from the permeate of reverse osmosis in the treatment plant in Emmen. The iron concentration in the effluent is targeted at <0.1 mg/L (De Pascale et al., 2013). The cause of the presence of iron in the produced water was hypothesized as follows:

1. Iron removal in the treatment plant is not sufficient due to a combination of a low temperature and a low pH of the water, which makes the oxidation of Fe(II) and formation of Fe(III) floc very slow, and thus the iron stays in Fe(II) form and passes through the sand filter.
2. The Fe(II) is oxidized to Fe(III), however, the size of the flocs is too small to be retained by the rapid sand filter.
3. The sand filter removes iron through adsorption of Fe(II) most of the time throughout the year, and there is an saturation of Fe(II) adsorption capacity of the filter media that leads to the breakthrough of Fe(II).

1.3.2. Research questions

To meet the research objectives, the following research questions are formulated:

1. Is the retention time of the tower aerator and the sand filter sufficient to allow full oxidation of the Fe(II), and flocculation of the Fe(III)?
2. Does changing the pH of the permeate affect the oxidation rate of Fe(II) into Fe(III) and hinders the formation of the flocs to a size of <0.2 µm?
3. To what extent does the concentration of nitrate in the permeate affect the oxidation rate of Fe(II) into Fe(III) and hinders the formation of the iron flocs to a size of <0.2 µm?
4. Can the rapid sand filter retain the iron flocs that are formed after Fe(II) oxidation and hydrolysis, and also remove Fe(II) through adsorption?
5. What are the options to increase pH to >7 to improve iron removal?

1.4.Structure of this report

The report is structured as follows. In chapter 2, background theory on the relevant information regarding iron removal from groundwater is presented. Subsequently, the materials and methods that are used to conduct the research are explained in Chapter 3. Next, Chapter 4 contains the results from the study and discussions of the results. Lastly, Chapter 5 contains the conclusions and recommendations.

2
Literature Review

2.1. Iron in Groundwater

Iron is commonly found in groundwater in certain concentrations depending on the geological condition of the location. The concentration in groundwater may range from few hundredths to about 50 mg/L (Hem, 1985). Under an anaerobic condition and the availability of reducing agents such as organic matter and hydrogen sulfide, iron in the rocks and minerals may dissolve and get into the groundwater. In groundwater, iron may exist in several forms depending on the pH and redox potential: a) dissolved as iron (II), b) inorganic complexes, c) organic complexes, d) colloidal, and e) suspended. From all of those forms, iron in groundwater is mostly found in the dissolved state of Fe(II) (Sharma, 2001).

2.2. Iron removal by sand filtration

Aeration followed by rapid sand filtration is a common treatment method to remove iron from groundwater in the Netherlands (Vries et al., 2017). Oxidation of dissolved Fe(II) will produce iron hydroxide. A long residence time of the aerated water before filtration allows the iron hydroxide to flocculate and be retained by the sand filter (Van Beek et al., 2012). In contrast, short oxidation time before sand filter allows the removal of iron through adsorption of Fe(II) to the sand particles to be more dominant (Van Beek et al., 2012)

2.2.1. Iron floc filtration

Filtration of iron flocs through rapid sand filtration can occur through several mechanisms such as straining, sedimentation, inertial impingement, interception, and diffusion that are visualized in figure 2.1. Straining will occur when the size of the particles is larger than the pore size of a filter. Straining can result in a cake surface on the top layer of the filter bed, which causes rapid head loss development and clogging.

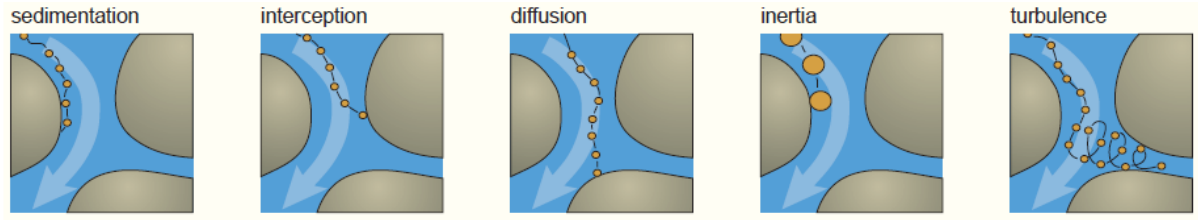

Figure 2. 1 Removal mechanism of particles in rapid sand filter
Note. Adapted from *Granular Filtration Dictaat* (p. 84), by TU Delft, 2004

To minimize clogging, pre-treatment is usually done in a water treatment plant by sedimentation or flotation, thus only small particles can enter the filter and flow through the pores (Bernardes, 2016; Cromphout et al., 2013; García-Ávila et al., 2020). Most of the suspended particles have a higher density than water and subjected to the effect of sedimentation. Moreover, particles that have sufficient momentum can impinge the sand grain due to inertia. Removal of particles can also occur through the

diffusion of particles into the surface of media, especially for lighter particles. When the trajectory of the particles is near the filter media, interception of the particles can occur (Saleh, 1981).

2.2.2. Adsorption and heterogeneous oxidation

Filter media such as sand has some capacity to adsorb Fe(II). The adsorption of Fe(II) onto media is influenced by several factors such as pH, other competing ions, and organic matters. Higher pH increases the sorption capacity of sand media, whereas other ions can either increase, decrease, or has no effect on Fe(II) adsorption depending on the ion (Sharma, 2001). With the presence of oxygen in the water, the adsorbed Fe(II) can then undergo oxidation and hydrolysis (Van Beek et al., 2012). The reactions are formulated as follows (Van Beek et al., 2012):

Fe(II) adsorption: $$S-OH^0 + Fe^{2+} \rightarrow S-OFe(II)^+ + H^+ \quad (2.1a)$$

Oxidation: $$S-OFe(II)^+ + \frac{1}{4}O_2 + H^+ \rightarrow S-OFe(III)^{2+} + \frac{1}{2}H_2O \quad (2.1b)$$

Hydrolysis: $$S-OFe(III)^{2+} + 2H_2O \rightarrow S-OFe(III)(OH)_2^0 + 2H^+ \quad (2.1c)$$

Overall: $$S-OH^0 + Fe^{2+} + \frac{1}{4}O_2 + 1\frac{1}{2}H_2O \rightarrow S-OFe(III)(OH)_2^0 + 2H^+ \quad (2.1)$$

Heterogeneous oxidation, which is characterized by adsorption of Fe(II) into filter media or iron hydroxide and oxidation of the adsorbed Fe(II) occurs mainly inside the filter bed. Over time, the adsorbed Fe(II) that has been oxidized will accumulate and increase the thickness of the filter bed due to the ability of iron oxide to also adsorb Fe(II) (Van Beek et al., 2016). The rate equation for heterogeneous oxidation is represented in equation 2.2 (Van Beek et al., 2016):

$$\frac{d}{dt}[Fe^{2+}] = -k_2 \frac{[S-OH^0][Fe^{2+}][O_2]}{[H^+]} \quad (2.2)$$

$[S\text{-}OH^0]$ = concentration of Fe(III) hydroxide (mol/L)
$[Fe^{2+}]$ = concentration of Fe(II) (mol/L)
$[H^+]$ = concentration of H+ (mol/L)
$[O_2]$ = concentration of dissolved oxygen (mol/L)
k_2 = rate constant for heterogeneous oxidation ($L.mol^{-1}.s^{-1}$)

2.3. Iron oxidation and hydrolysis

Oxidation and filtration is the most common method to remove iron from water. Iron in the form of Fe(II) is dissolved in water and can be oxidized to Fe(III). The oxidation reaction is shown in equation 2.3:

$$4Fe^{2+} + O_2 + 2H_2O \rightarrow 4Fe^{3+} + 4OH^- \quad (2.3)$$

After oxidation, the Fe(III) hydroxide commonly form and can subsequently flocculate and easily be removed by filtration (Sommerfeld, 1999). The oxidation of dissolved Fe(II) and its subsequent hydrolysis and precipitation of hydrous ferric oxide are commonly known as homogeneous oxidation (Van Beek et al., 2016). The rate equation for homogeneous oxidation may be represented as (Sung & Morgan, 1980):

$$\frac{-d[Fe(II)]}{dt} = k_a \; pO_2 \; [Fe(II)]\,[OH^-]^2 \quad (2.4)$$

Where:

$-d[Fe(II)]/dt$	= Fe^{2+} oxidation rate (mol/L.s)
k_a	= reaction rate constant ($L^2\ mol^{-2}\ atm^{-1}\ s^{-1}$)
$pO2$	= partial pressure of oxygen (atm)
$[Fe(II)]$	= concentration of ferrous iron (mol/L)
$[OH^-]$	= concentration of hydroxyl ions (mol/L)

2.3.1. Influence of pH

As can be seen from equation 2, the oxidation rate of Fe(II) is highly influenced by pH, increasing 100 times for each 1 unit increase in pH. The effect of pH on the oxidation of Fe(II) is shown in **Figure 2. 2** (Stumm & Lee, 1961). However, when the pH of water is higher than 7, the oxidation of Fe(II) becomes heterogeneous. Heterogeneous Fe(II) oxidation is characterized by adsorption of Fe(II) into the surface of Fe(III) hydroxides (Van Beek et al., 2016).

Initially, homogenous oxidation takes place and Fe(III) is formed. The formation of iron hydroxides provides a surface where autocatalyzing of Fe(II) oxidation can take place. As more iron hydroxides are formed, autocatalytic oxidation becomes more important due to the attraction of OH^- into the diffuse layer that makes pH on the diffuse layer of Fe(III) flocs higher than the bulk solution (Sung & Morgan, 1980; Tamura et al., 1976b; Tüfekci & Sarikaya, 1996).

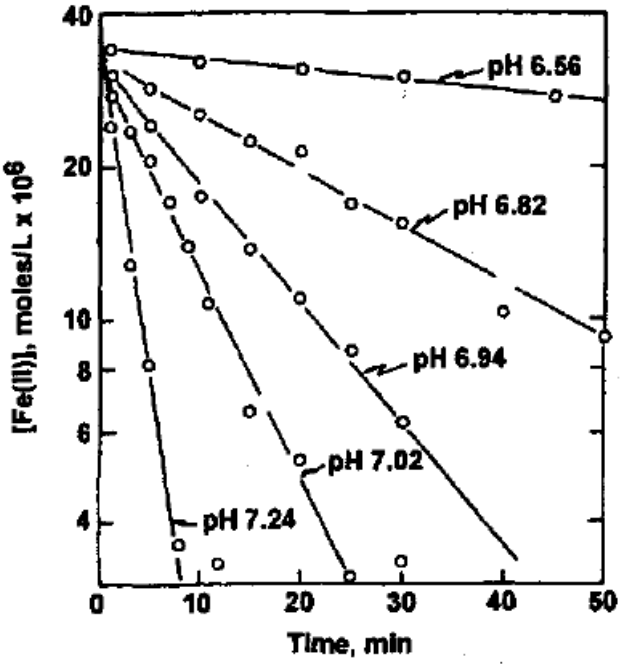

Figure 2. 2 Effect of pH on the oxidation of Fe(II) (Stumm & Lee, 1961)

2.3.2. Influence of temperature

Aside from pH, oxidation of Fe(II) into Fe(III) is also influenced by temperature. It has been observed that the oxidation rate increases 10 times with an increase of temperature of 15ºC. The influence of temperature can be attributed to the variation of OH^- ion activity with temperature for a given pH, as a result of temperature variation in K_w. (Stumm & Lee, 1961; Sung & Morgan, 1980). The effect of temperature on the oxidation of Fe(II) is shown in **Figure 2. 3**.

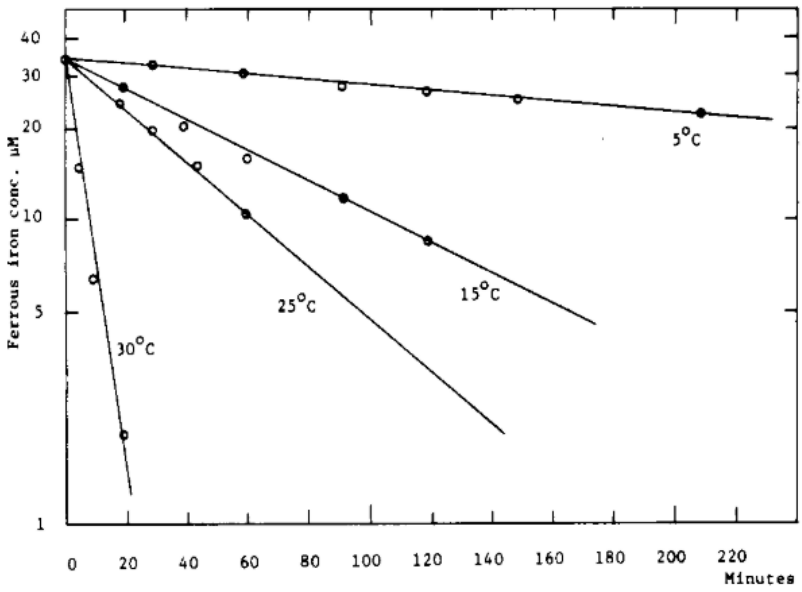

Figure 2. 3 Effect of temperature on the oxidation of Fe(II) at pH ~6.82 (Sung & Morgan, 1980)

2.3.3. Influence of ions

The effects of several anions (ClO_4^-, NO_3^-, Cl^-, Br^-, I^-, SO_4^{2-}, $H_3SiO_4^-$, F^-, and $H_2PO_4^-$) on the oxidation of Fe(II) has been studied (Tamura et al., 1976a). The oxidation rate with the presence of perchlorate, nitrate, silicate, bromide, iodide, and sulfate is lower compared to the oxidation rate without their presence. In contrast, the presence of fluoride and phosphate ions accelerates the oxidation reaction (Tamura et al., 1976a).

Moreover, the oxidation rate of Fe(II) is also dependent on ionic strength. It was found that increasing ionic strength also increases the half-time for iron oxidation, slowing down the oxidation reaction. The relation of ionic strength with oxidation rate constant is described with the linear regression equation $\log k = 13.76 - 2.06\sqrt{I}$ with k in units of M^{-2} atm^{-1} min^{-1} at a temperature of 25°C and alkalinity of 9 mmol/L HCO_3^- (Pullin & Cabaniss, 2003; Sung & Morgan, 1980).

The characteristic of precipitate is also influenced by the presence of ions in groundwater such as silicate, phosphate, arsenic, and calcium. By binding strongly to precipitate surfaces, phosphate and silicate can inhibit crystal growth, leading to poorly-ordered solids (Kaegi et al., 2010; Senn et al., 2018). Moreover, phosphate and silicate can also decrease the particle surface charge, which strongly influences particle aggregation, making the oxidized iron stay in suspension and hinder the filtration (Dart & Foley, 1970; Sposito, 2008).

2.3.4. Influence of alkalinity

It was found in one study that changes in bicarbonate concentration from 0.002M to 0.01M do not change the oxidation rate of Fe(II) when the pH during the oxidation experiment is kept constant (Tamura et al., 1976a). However, bicarbonate plays a role during hydrolysis. As hydrolysis occurs, H^+ ion is produced (eq. 2.5). The H^+ will react with HCO_3^- and shift the bicarbonate equilibrium, resulting in a slight decrease in pH (Lerk, 1965). The buffering capacity of bicarbonate prevents excessive pH drops, and in return can maintain the oxidation rate of Fe(II).

2.3.5. Fe(III) hydrolysis and floc formation

After oxidation, the formed Fe(III) undergoes hydrolysis and subsequently forms hydrated iron oxide ($Fe_2O_3.xH_2O$). The reactions are (Lerk, 1965):

$$4Fe^{2+} + O_2 + 2H_2O \rightarrow 4Fe^{3+} + 4OH^- \quad (2.5a)$$

$$4Fe^{3+} + 4OH^- + 2(x+1)H_2O \rightarrow 2(Fe_2O_3xH_2O) + 8H^+ \quad (2.5b)$$

Combined, the overall reaction becomes:

$$4Fe^{2+} + O_2 + 2(x+4)H_2O \rightarrow 2(Fe_2O_3xH_2O) + 8H^+ \quad (2.5)$$

The hydrolyzed iron will form dimers that may hydrolyze further providing additional hydroxo bridges. Subsequently, polynuclear hydroxy complexes may form and ultimately form precipitates (Sharma, 2001). The ability of these precipitates to rapidly flocculate will depend on the charges of the particles. Stabilization of Fe(III) through complexation with organic acids, for example, can slow the rate of iron floc formation (Pullin & Cabaniss, 2003). For iron removal through floc filtration, well flocculated ferric hydroxide suspensions are very important because colloidal particles are too small to be easily removed (Gregory, 1984).

3
Materials and Methods

3.1. Materials

Synthetic permeate water was used to conduct the experiments. The composition of the synthetic water was made following the characteristic of the real permeate in the treatment plant. The reference composition of the synthetic water is shown in **Table 3. 1**.

The stock solutions for Fe(II) and Mn(II) were prepared by dissolving $FeSO_4.7H_2O$ and $MnCl_2$ salt respectively in demineralized water. To prevent the oxidation of both Fe(II) and Mn(II), HCl was added to acidify the solution to pH 2 that will slow down the oxidation considerably. The stock solutions for HCO_3, NO_3, P, and Ca were prepared by dissolving $KHCO_3$, $NaNO_3$, $NaH_2PO_4.H_2O$, and $CaCl_2$ respectively in demineralized water. All of the salts are reagent grade and were obtained from Sigma Aldrich.

Table 3. 1 Reference composition of synthetic water (units in mmol/L)

Component of real permeate	Values	Component of synthetic water	Value
pH	5.7 – 6.2	pH	6
Fe(II)	0.02 – 0.03	$FeSO_4$	0.021
Mn(II)	0.0007 – 0.001	$MnCl_2$	0.001
HCO_3^-	0.61 – 1.1	$KHCO_3$	1
NO_3^-	0.1 – 0.2	$NaNO_3$	0.2
Ca^{2+}	0.2	$CaCl_2$	0.2
Cl^-	0.1 – 0.5		
Na^+	0.2 – 0.6		
K^+	<0.1		

Note: Components of the real permeate was the result of permeate characteristics measurement by Hatenboer-Water, 2020

3.2. Methods

3.2.1. Phreeqc iron oxidation simulation

To better understand the iron oxidation kinetics, simulation using Phreeqc was done. Phreeqc is a modeling program that is designed to perform aqueous geochemical calculations. The oxidation model itself was developed following Example 9 “Kinetic Oxidation of Dissolved Ferrous Iron with Oxygen” that was provided with the program (Parkhurst & Appelo, 1999).

The input for Phreeqc is categorized into several data blocks using a specific keyword. For modeling homogenous iron oxidation, the keyword data blocks that were used are:

1. **SOLUTION_MASTER_SPECIES** keyword was used to define the element Fe(II) and Fe(III) species.
2. **SOLUTION_SPECIES** keyword was used to define the chemical reactions that happen during oxidation reaction.

3. **SOLUTION** keyword was used to define the chemical composition of the initial solution that also includes temperature and pH. The chemical composition inputted to Phreeqc was based on the characteristics of permeate from the water treatment plant in Emmen.
4. **RATES** keyword was used to define the mathematical equation for the kinetic reaction of homogenous iron oxidation. The reaction rate for homogenous iron oxidation is described by the kinetic rate that is valid for pH interval 5 to 8 (Sung & Morgan, 1980):

$$\frac{d}{dt}[Fe^{2+}] = -k_{Fe,hom}\, pO_2 [Fe^{2+}][OH^-]^2 \qquad (3.1)$$

   The reaction rate constant is dependent on temperature, presence of interfering cations and anions, organic matters, and buffering capacity (Jobin & Ghosh, 1972; Stumm & Lee, 1961; Sung & Morgan, 1980). For this modeling, a reaction rate coefficient *k* of 1.33 x 10^{12} (L^2 mol^{-2} atm^{-1} s^{-1}) (Tamura et al., 1976a) was used, and adjustment to the rate coefficient was made to fit the model with the oxidation experiment.
5. **KINETICS** keyword was used to specify the kinetic reaction of iron oxidation and define the stoichiometric coefficient of the iron oxidation reaction.

3.2.2. Oxidation and precipitation experiment

The experiments were carried out with 1L beaker glass and stirred by using jar test apparatus (Velp Scientifica). A multimeter was used to monitor the relevant parameters during the oxidation experiment, namely pH, dissolved oxygen, and redox potential. The apparatus setup is illustrated in **Figure 3.1**. To simulate groundwater temperature of about 12°C, the experiments were done in the climate room of Stevin II laboratory which has a controlled room temperature of around 10.3°C – 11°C. It should be noted that the temperature of the climate room is lower than the real groundwater. However, it was assumed that the temperature difference was little and would not impact the oxidation of Fe(II) much.

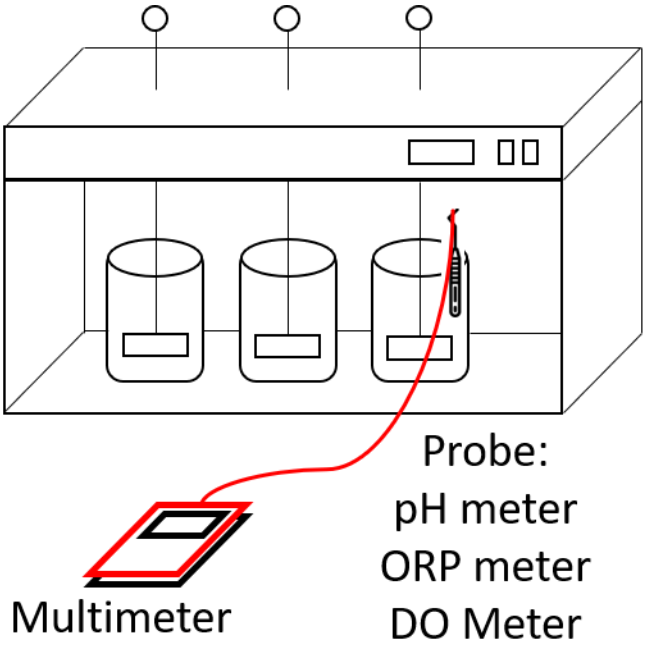

Figure 3. 1 Schematic diagram of oxidation experiment using jar test equipment

The synthetic permeate was prepared by using demineralized water that already had an O_2 concentration of 10 – 11 mg/L. As the oxygen requirement to oxidize 20 µmol/L of Fe(II) is only 0.1 mg/L, no additional oxygen sparging was needed. Before the oxidation experiment started, the synthetic permeate without Fe(II) and Mn(II) was prepared first. The composition of the synthetic permeate is shown in

Table 3.2. The experiment was started once the desired volume of Fe(II) stock solution is put into the beaker glass. The beaker glasses that were used in the experiment were equipped with baffles.

Table 3. 2 Composition of solutions that were used during the oxidation experiment (concentration in mmol/L)

Experiment	Initial solution composition						
	Initial pH	$FeSO_4$	$MnCl_2$	$KHCO_3$	$NaNO_3$	$CaCl_2$	NaH_2PO_4
pH-6	6	0.021	0.001	1	0.2	0.2	-
pH-7	7	0.021	0.001	1	0.2	0.2	-
pH-8	8	0.021	0.001	1	0.2	0.2	-
NO_3^- 0.04	8	0.021	0.001	1	0.04	0.2	-
NO_3^- 0.4	8	0.021	0.001	1	0.4	0.2	-
HCO_3^- 0.5	8	0.021	0.001	0.5	0.2	0.2	-
HCO_3^- 2	8	0.021	0.001	2	0.2	0.2	-
$NaH_2PO_4^-$ 0.04	8	0.021	0.001	1	0.2	0.2	0.04

The experiments lasted for 60 minutes. In the first 5 minutes of the experiment, the stirring speed was set to 120 rpm, and after that lowered to 80 rpm. A fast stirring speed of 120 rpm in the first 5 minutes was used to rapidly mix the solution, and the slower 80 rpm was used to avoid turbulence and allow the iron flocs to form. The first sample was taken at the start of the experiment without filtering the sample. The next samples were taken every 10 minutes and filtered through a 0.2 µm filter. The samples were then preserved by adding 1 drop of reagent Fe-1 from Spectroquant Iron Test 1.00796 that contains 10% HNO_3 (Merck, 2007) to quench the oxidation of Fe(II).

3.2.3. Iron floc sand filtration experiment

The column experiment was done to simulate the removal of iron floc by rapid sand filtration. The apparatus setup for the column filtration experiment is shown in **Figure 3. 2**. The setup consists of three main components: a beaker for mixing, a peristaltic pump, and a filter column. The beaker was used to mix the solutions. In addition, the oxidation of Fe(II) and flocculation of iron hydroxide also took place in the beaker.

The peristaltic pump was used to pump the water from the beaker to the column filter. The pump was operated at 81 rpm that corresponds to a flowrate of 78 mL/minute. The inner diameter of the column was 3.4 cm, and the column was filled with new natural silica sand until the height of 20 cm. The new sand was procured from Hatenboer-Water and has a size of 0.40 – 0.80 mm. Before the experiment was started, the column was flushed with demineralized water to remove dirt that may contribute to the turbidity of the filtrate and interfere with the measurement of iron concentration through spectrophotometry. The filter was operated with a flow rate of 78 mL/minute that corresponded with a filtration velocity of 5.2 m/hour.

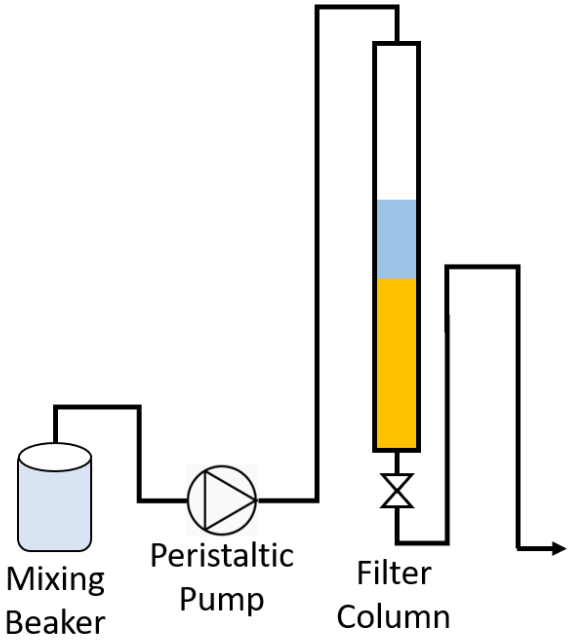

Figure 3. 2 Column filtration setup illustration

The first experiment was conducted to investigate the effect of nitrate on the filtration of iron floc. The nitrate concentration of the solution was varied between 0.2 mmol/L and 0.4 mmol/L. The experiment was conducted in triplicate for each nitrate concentration. Before the solution was filtered through the column, it underwent oxidation for 45 minutes at initial pH of 8 to completely oxidize the Fe(II) into Fe(III). After the oxidation was finished, two samples were then taken and filtered through a 0.2 µm and 0.45 µm syringe filter to discern the particle size of the formed iron flocs. Then, the solution was filtered through the column. The filtrate was then sampled twice. The first sample was sampled without filtering, and the second sample was filtered through a 0.2 µm syringe filter.

The second experiment was conducted to investigate the clogging of the sand filter and breakthrough of iron through the sand filter. Before the experiment was conducted, the column was backwashed to clean the filter bed from the iron floc from the previous experiment. As with the previous experiment, the Fe(II) solution was stirred in a separate 1L beaker glass for about 30 minutes to be fully oxidized before being pumped into the column. After 30 minutes, the solution was pumped into the sand filter at a flow rate of 78 mL/minute. Samples were taken before the water passed through the column for turbidity measurement. After the water passed through the column, samples were taken for turbidity measurement and Fe total analysis.

3.2.4. Fe(II) adsorption by sand filter breakthrough

This experiment was conducted to investigate the breakthrough of Fe(II) when the column sand filter was operated to adsorb Fe(II) instead of filtering iron flocs. The column was cleaned from any previous iron flocs by backwashing it before the experiment began. The pH of the solution was adjusted to about 6 to mimic the pH of the permeate after aeration. The demineralized water was already saturated with oxygen, thus no additional air sparging was needed. The Fe(II) was added into the solution and mixed for a few seconds and then the solution was pumped into the column sand filter at a flow rate of 78 mL/minute. Samples were taken before and after filtration at a time interval of 30 minutes and then analyzed for Fe(II).

3.2.5. COMSOL adsorption breakthrough simulation

The result of the Fe(II) adsorption breakthrough from the column experiment could not be directly translated into the breakthrough of a full-scale rapid sand filter. COMSOL was used to model the breakthrough of Fe(II) adsorption through the column and to predict the Fe(II) adsorption breakthrough in a full-scale rapid sand filter. An adsorption breakthrough model (Hu, 2020) has been developed before and that model was used in this study.

The model was based on a one-dimensional mass transfer model. In this model, the concentration of Fe(II) in the effluent was influenced by convective mass transfer, axial dispersion, and adsorption by adsorbent (Hu, 2020). Adsorption reactions are typically rapid and are assumed to be mass transfer controlled. The removal of iron by adsorption can be described by the macroscopic mass conservation equations (Hu, 2020; Sharma, 2001):

$$\frac{\partial c}{\partial t} = D_L \frac{\partial^2 c}{\partial z^2} - v\frac{\partial c}{\partial z} - \rho\left[\frac{1-\varepsilon}{\varepsilon}\right]\frac{\partial q}{\partial t} \tag{3.2}$$

The adsorption rate by adsorbent was postulated to be linearly proportional to the driving force, which is the difference between the surface concentration and the average adsorbed phase concentration (Sharma, 2001). The solid phase mass balance is described mathematically by the linear driving force (LDF) equation:

$$\frac{\partial q}{\partial t} = k(q_s - q) \tag{3.3}$$

The Freundlich isotherm equation was used for equilibrium:

$$q_s = K_F\, {c_s}^n \tag{3.4}$$

Where,

- c = concentration of Fe(II) in water (mg/L)
- c_s = concentration of Fe(II) near the surface of adsorbent (mg/L)
- D_L = dispersion coefficient (m^2/s)
- v = superficial velocity of water (m/s)
- ρ = density of sand media (kg/m^3)
- ε = bed porosity (-)
- q = (amount of Fe(II) adsorbed) / (amount of adsorbent) (kg/kg)
- q_s = (amount of Fe(II) adsorbed that is in equilibrium with the concentration of Fe(II) near the surface of adsorbent) / (amount of adsorbent) (kg/kg)
- z = longitudinal distance in the column (m)
- t = time (s)
- k = LDF kinetic rate coefficient (s^{-1})
- K_F = Freundlich adsorption constant [$(mg/g)/(mg/m^3)^n$]
- n = Freundlich empirical coefficient (-)

Then, the equations 3.2 – 3.4 were entered in COMSOL in dimensionless form (Hu, 2020):

Overall mass balance equation:

$$-\frac{1}{Pe}\frac{\partial^2 x}{\partial l^2} + \frac{\partial x}{\partial l} + \frac{\partial x}{\partial t} + D_g\frac{\partial y}{\partial t} = 0 \tag{3.5}$$

Kinetics equation:

$$\frac{\partial y}{\partial t} = S(y^* - y) \tag{3.6}$$

Isotherm equation:

$$y^* = \frac{K_F(c_0 x)^n}{q_0^*} \tag{3.7}$$

The parameters that need to be inputted and their numerical values are shown in **Table 3. 3**. The parameters *k*, K_F, and *n* relate to the adsorption isotherm and kinetics of Fe(II) into the sand particle. The values of the parameters were adjusted by trial and error in COMSOL to fit the model with the results of the experiment. The values of K_F, *n*, *k*, and D_L were taken from a previous Fe(II) adsorption study by Sharma (2001). The parameters ρ, ε, and L relates to the properties of the sand in the sand column. The values of ρ and ε were assumed.

Table 3. 3 Values of input parameters for COMSOL adsorption breakthrough model

Parameters	Value	Description
k	2.6×10^{-4} /s	LDF kinetic rate coefficient
K_F	2.3×10^{-3} [(mg/g)/(mg/m^3)^n]	Freundlich isotherm constant
n	0.54	Freundlich empirical coefficient
D_L	1.6×10^{-4} m^2/s	Dispersion coefficient
c_0	0.02 mol/m^3	Fe(II) inflow concentration
ρ_b	1560 kg/m^3	Bulk density of sand
ρ_p	2600 kg/m^3	Particle density of sand
ε	0.4	Bed porosity
L	0.2 m	Column length
v	5.2 m/h	Interstitial velocity

3.3. Analysis

3.3.1. Iron concentration measurement

The iron concentrations were measured using Merck Spectroquant 1.00796.0001 Iron Test kit. The analytical measurement of this test kit is based on the 1-10 phenanthroline method that forms a red complex that is then measured photometrically. The test kit consisted of three different reagents termed Fe-1, Fe-2, and Fe-3. Reagent Fe-1 and Fe-2 were used to determine Fe(II) in the sample, and if total Fe was needed to be determined, reagent Fe-3 was also used. The kit has a measuring range of 0.01 – 5.00 mg/L.

To prepare for iron analysis, 8 mL of sample was taken from the stirred solution and transferred into a tube. Then, one drop of reagent Fe-1 was added to the sample. After that, 0.5 mL of reagent Fe-2 was pipetted into the tube. After mixing, the sample was left for 5 minutes to react. To measure the Fe(II), the samples were put into cuvettes and then measured spectrophotometrically using Spectroquant® NOVA 60A.

To determine the total iron, 1 dose of reagent Fe-3 was added to the tube after the reaction of reagent Fe-1 and Fe-2 was finished. Reagent Fe-3 contains ascorbic acid that reduces all Fe(III) into Fe(II). The sample tube was then shaken until the reagent was completely dissolved. The sample was then left for 10 minutes to react before it was measured spectrophotometrically. The concentration of Fe(III) in the sample was calculated by subtracting the measured Fe(II) concentration from the total Fe concentration.

3.3.2. Turbidity

Turbidity was measured using Hach 2100N Turbidity Meter in the NTUs unit. Before the measurement of samples was conducted, the measurement of the machine was checked using the standard solution of 1000 NTU, 200 NTU, 20 NTU, 2 NTU, and <0.1 NTU. After that, the samples were transferred into the test tube and put into the turbidity meter. The machine automatically measures the turbidity of the sample.

4
Results and Discussions

4.1. Effects of several parameters on Fe(II) oxidation and iron floc formation

The iron removal process by floc filtration is affected by several parameters such as pH and ions. In this section, the effect of pH, nitrate, and bicarbonate on iron removal by floc filtration was investigated by conducting batch oxidation experiments to oxidize Fe(II) and hydrolyze the Fe(III) into iron floc.

4.1.1. Effect of pH on iron oxidation

Increasing pH can accelerate the oxidation of Fe(II) into Fe(III) (Stumm & Lee, 1961). However, the finding from previous studies cannot be directly used to determine the oxidation of iron in the case of Emmen because of differences in characteristics of the water. Thus, the experiment to study the effect of pH was conducted with synthetic water that closely resembled the characteristics of the permeate in Emmen to better understand the effect of pH on the oxidation of iron in the Emmen case.

The effect of pH on the oxidation of iron was investigated by varying the initial pH (pH_{init}) of the synthetic water at pH 6, 7, and 8. The speciation of the Fe(II) and the oxidized product, Fe(III) was also done by filtering the sample through a 0.2 µm syringe filter. The temperature during the experiment was relatively constant in the range of 10.3°C – 10.6°C. The effect of pH on Fe(II) oxidation is shown in **Figure 4. 1**.

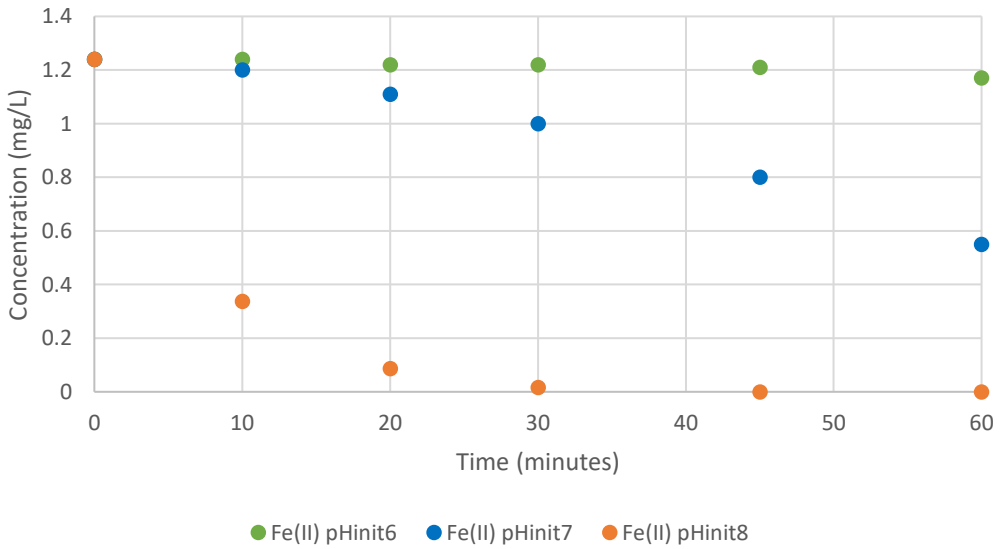

Figure 4. 1 Concentration of Fe(II) over time during oxidation in batch experiments at pH_{init} 6 (green), 7 (blue), and 8 (orange)

The experiment at pH_{init} of 6 resulted in slow oxidation of Fe(II). With an initial Fe(II) concentration of 1.24 mg/L, only 4.4% of the Fe(II) was oxidized in 60 minutes, reaching an end concentration of 1.20 mg/L. The experiments at pH_{init} of 7 and 8 were done to determine the effect of increasing pH on the oxidation of Fe(II) in the permeate. It was found that the oxidation rate of iron is more rapid in the water with higher initial pH, which confirmed the finding of previous studies (Stumm & Lee, 1961). In

solution with pH_{init} of 8, the Fe(II) reached 0.02 mg/L (98.7% oxidized) after 30 minutes. In solution with pH_{init} of 7, the Fe(II) reached 0.57 mg/L (54% oxidized) after 60 minutes.

However, the result from the experiment could not be compared directly to the result of previous studies (El Azher et al., 2008; Stumm & Lee, 1961; Sung & Morgan, 1980; Tamura et al., 1976a), because of the differences in the experimental condition and water composition. In this experiment, the pH of the solution was not kept constant (see **Figure 4. 3**), whereas the pH in the previous studies is maintained constant. The initial Fe(II) concentrations of the previous studies are also higher, at 10 mg/L (El Azher et al., 2008), and 2 mg/L (Stumm & Lee, 1961; Sung & Morgan, 1980). Moreover, the temperatures of the experiment are also different, at 20ºC (El Azher et al., 2008; Stumm & Lee, 1961) and 25ºC (Sung & Morgan, 1980).

To better compare the result from previous studies and this experiment, Phreeqc was used to simulate the oxidation of Fe(II) using a rate coefficient of 1.33×10^{12} ($L^2\ mol^{-2}\ atm^{-1}\ s^{-1}$) (Tamura et al., 1976). However, the rate coefficient that was acquired from Tamura (1976) is the result of an experiment at a temperature of 25ºC. It was expected that using that rate coefficient will generate faster oxidation because the temperature in this study was in the range of 10.3ºC – 10.6ºC.

As expected, it was found that using the rate coefficient from Tamura (1976) produced an oxidation rate that was higher than the one observed in the experiment. At initial pH of 7, the simulation resulted in 61% of oxidation after 60 minutes compared to 54% in the experiment. At initial pH of 8, the simulation resulted in a higher oxidation rate. After 10 minutes, the Fe(II) in the simulation reached 0.02 mg/L, whereas 30 minutes was needed during the experiment to reach that level.

To better simulate the experimental condition, adjustment to the constant rate used in Phreeqc was done by trial and error. The new constant rate was set to 5.4×10^{11} ($L^2\ mol^{-2}\ atm^{-1}\ s^{-1}$), which is 0.41x slower than the previous constant rate. According to Sung & Morgan (1980), the half-life of Fe(II) at 15ºC is 0.60x the half-life at 25ºC. Since the oxidation rate at a lower temperature is slower, the oxidation rate at approx. 10.5ºC should be lower than 0.60x. Thus, the oxidation rate of 0.41x seems to be in the ballpark. Thus, it can be concluded that the lower oxidation rate of the experiment compared to Tamura's rate was mainly due to the lower temperature during the experiment.

Aside from temperature, the difference in oxidation rate between the experiment in this study and previous studies was also contributed from the differences in ionic composition and ionic strength of the water. The most obvious difference was in the bicarbonate concentration. In this study, the concentration of bicarbonate was 1 mmol/L. In contrast, it is 9 mmol/L in Sung & Morgan (1980) and 10 mmol/L in Tamura (1976).

The comparison of simulated Fe(II) oxidation using the new constant rate and the experiment is shown in **Figure 4. 2**. At pH_{init} of 6 and 7, the oxidation rate of Phreeqc was approximately the same as that of the experiment in the first 30 minutes. However, whereas the oxidation rate of Phreeqc remained relatively constant beyond 30 minutes, the oxidation rate of the experiment became faster.

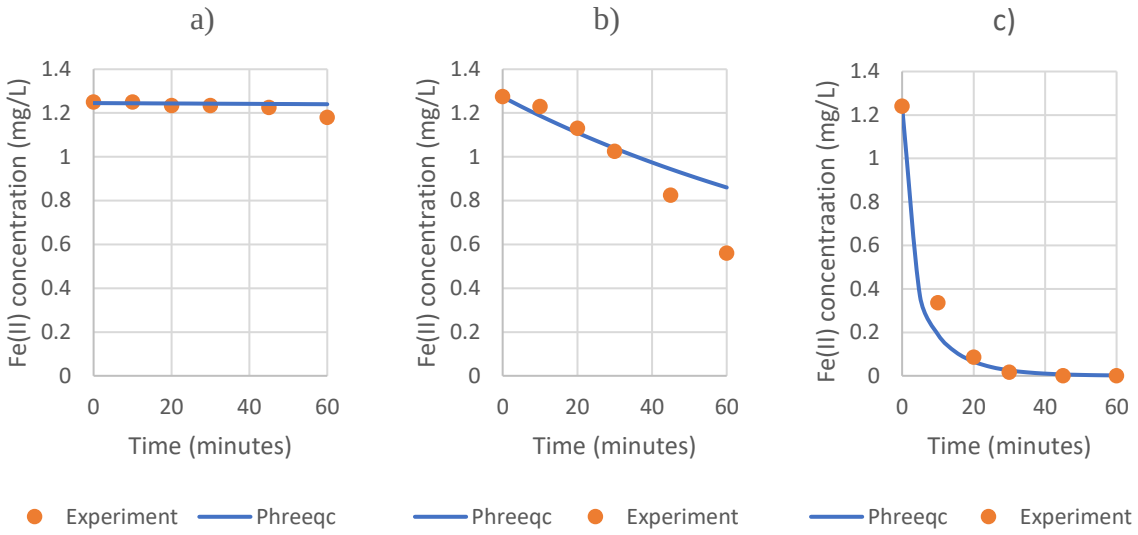

Figure 4. 2 Concentration of Fe(II) over time during oxidation experiment and simulation at a) pH_{init} 6, b) pH_{init} 7, c) pH_{init} 8

The difference could be linked to the differences in changes of pH between the simulation and experiment that are shown in **Figure 4. 3**. In the experiment at pH_{init} of 6 and 7, the pH was always increasing reaching a final pH of 6.78 and 7.17, respectively, after 60 minutes. In contrast, the pH for pH_{init} 6 and 7 was always decreasing slightly in the simulation, reaching a final pH of 6.97 and 5.99, respectively. At pH_{init} of 8, the final pH was 7.6 in the experiment and 7.57 in the simulation, which is lower than the pH_{init}.

The increase in pH during the experiment at pH_{init} of 6 and 7 made the oxidation went faster, which is depicted by the concave shape of the points in **Figure 4. 1**. The decrease in pH in the experiment with pH_{init} of 8 was expected because, during oxidation of Fe(II) and its subsequent hydrolysis, H^+ ions are formed.

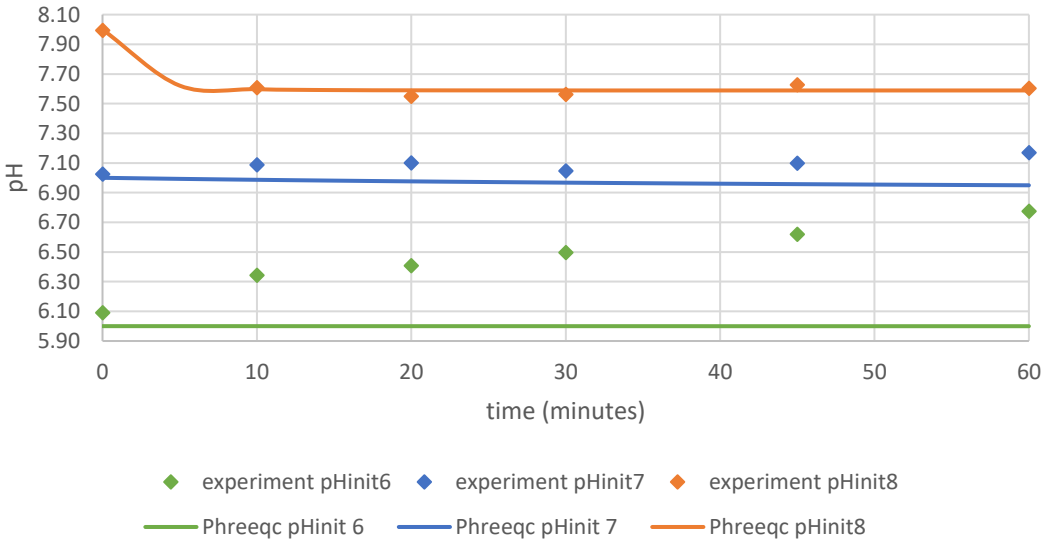

Figure 4. 3 pH changes during oxidation experiment and simulation at pH_{init} of 6, 7, and 8

The oxidation experiment was conducted using a jar test that was open to the atmosphere. During stirring of the solution, the transfer of gases between the atmosphere and the solution could have

happened. It was observed that the oxygen concentration during the experiment was always increasing. Thus, the increase in pH during the experiment might be due to the stripping of CO_2 that was more pronounced compared to the release of H^+ as a result of Fe(II) oxidation and the subsequent hydrolysis. In contrast, the Phreeqc software model geochemical reaction in a subsurface environment where contact between the solution and outside gases was limited. The stripping of CO_2 was not simulated and the decrease in pH in the simulation as a result of the release of H^+ ions during Fe(II) oxidation and hydrolysis can be observed.

An oxidation experiment was also conducted with the real permeate that had a pH_{init} of 5.76. Compared to the oxidation of Fe(II) in the synthetic water at pH_{init} of 6, the oxidation of Fe(II) in the real permeate was slightly faster, as can be seen in **Figure 4. 4**.

This might be due to the difference in cations/anions composition of the water. It was not possible to accurately create synthetic water that had the same characteristic as the real permeate. Aside from that, the real permeate already contained a small amount of Fe(III) that when hydrolyzed could adsorb Fe(II).

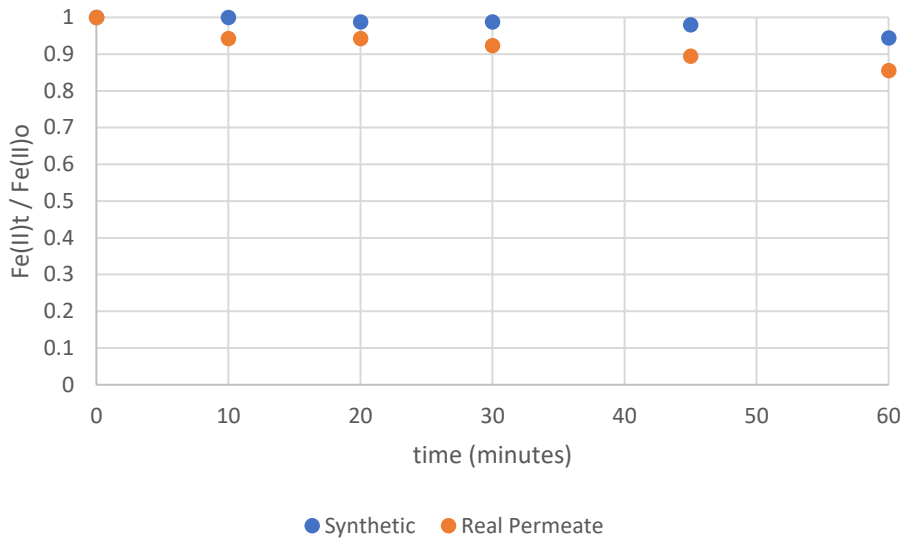

Figure 4. 4 Comparison of Fe(II) oxidation between synthetic water and real permeate at pH_{init} of 6

After the oxidation of Fe(II), the Fe(III) seemed to be readily hydrolyzed and precipitated. The speciation of Fe during the oxidation experiment was done by filtering through a 0.2 µm filter and the measurement is shown in **Figure 4. 5**. The figure shows the speciation of Fe(II), Fe(III) that had a particle size of <0.2 µm, and Fe(III) that has a particle size of >0.2 µm. Since the size of most of the Fe(III) was>0.2 µm the flocculation of iron seemed to be not retarded.

As oxidation of Fe(II) was more rapid at higher pH, more Fe(III) is formed. Consequently, more flocs were formed at higher pH because there were more Fe(III) available to be hydrolyzed. Thus, floc formation can be made more rapid by increasing the pH of the solution. Although there is no problem with flocculation, a filtration experiment with a sand filter is needed to conclude whether the flocs can be filtered by a sand filter or not.

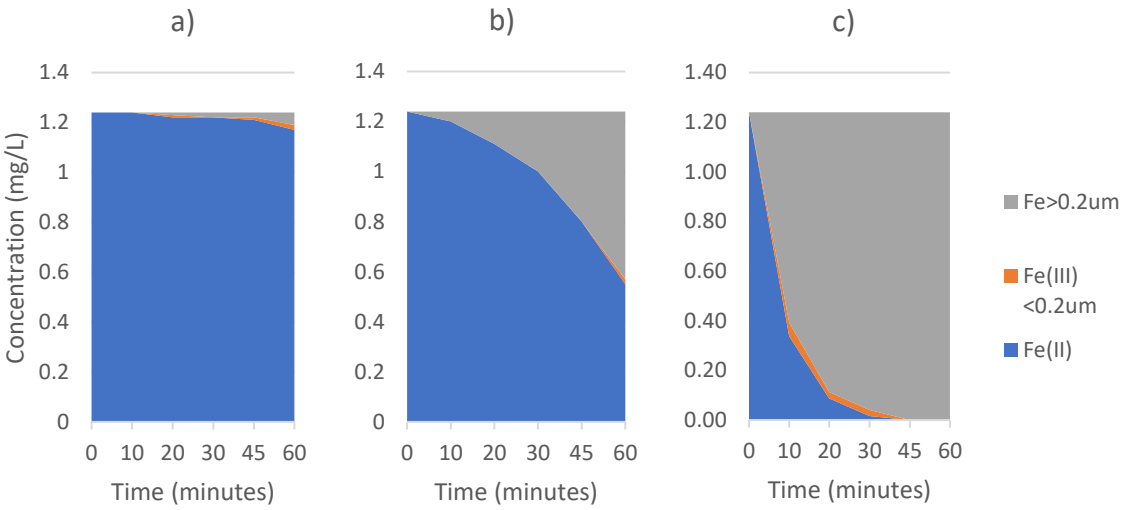

Figure 4. 5 Speciation of Fe during oxidation experiment at a) pH_{init} 6, b) pH_{init} 7, and c) pH_{init} 8

This oxidation experiment showed that oxidation of Fe(II) into Fe(III) was highly dependent on pH which confirmed previous studies. Faster oxidation can be achieved by increasing the pH of the water. However, whether iron removal can be achieved through floc filtration in the treatment plant will also depend on the retention time after the tower aeration and before the sand filter.

4.1.2. Effect of NO_3^-

In one measurement, the concentration of nitrate in the groundwater is 149 mg/L and is reduced to 12 mg/L by the RO membrane. It was previously hypothesized that the relatively high concentration of NO_3^- of 12 mg/L might hinder the oxidation of Fe(II) into Fe(III). To test this hypothesis, the effect of NO_3^- on the oxidation of Fe(II) was studied by varying the concentration of NO_3^- at 24 mg/L, 12 mg/L, and 2 mg/L. The experiment was conducted at a pH_{init} of 8. The results for the oxidation of Fe(II) with varying NO_3^- concentrations are shown in **Figure 4. 6**.

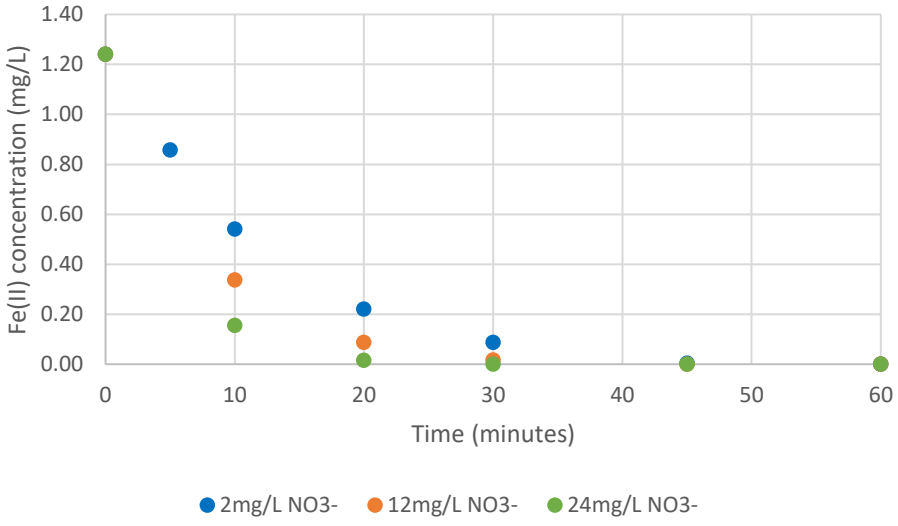

Figure 4. 6 Concentration of Fe(II) over time during oxidation experiment with different NO_3^- concentration

It was found that a higher NO_3^- concentration slightly accelerates the oxidation of Fe(II). In solution with 24 mg/L NO_3^-, the concentration of Fe(II) was 0.02 mg/L (98.8% oxidized) after 20 minutes of oxidation. In solution with 12 mg/L NO_3^-, it took 10 minutes longer to reach 0.02 mg/L of Fe(II). The concentration of Fe(II) was 0.02 mg/L after 30 minutes of oxidation. Although the differences in oxidation rate were not large, a t-test with a 99.5% level of confidence revealed that there was a significant difference between the oxidation rate of different nitrate concentrations.

After taking a closer look at the changes in pH during the experiment, the pH seemed to contribute to the oxidation rate for each NO_3^- concentration. **Figure 4. 7** shows the changes in pH during the oxidation experiment at different nitrate concentrations. At the nitrate concentration of 24 mg/L, the pH was higher than the other concentration. This might explain why the oxidation went faster for the solution with the nitrate concentration of 24 mg/L. In contrast, the pH at the nitrate concentration of 2 mg/L was the lowest compared to the others. This might explain why the oxidation went slower for the solution with the nitrate concentration of 2 mg/L

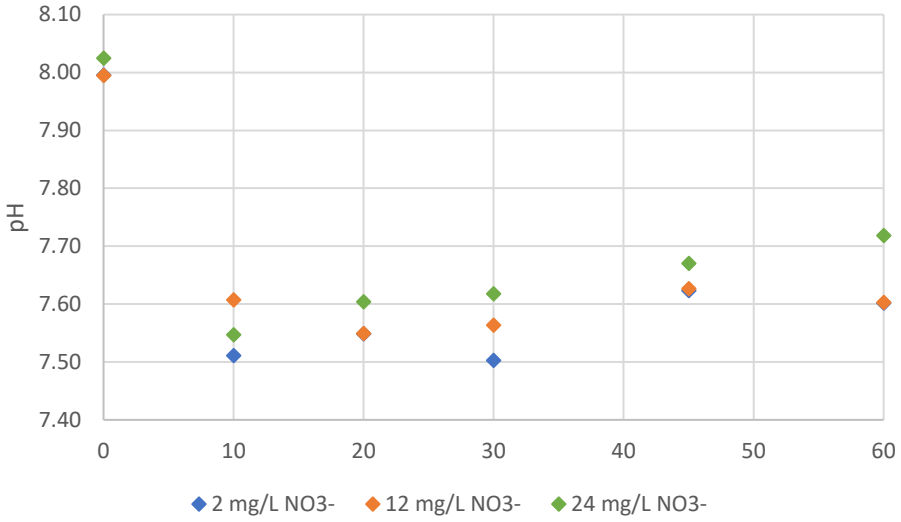

Figure 4. 7 Changes of pH during oxidation experiment at NO_3^- concentration of 2 mg/L, 12 mg/L, and 24 mg/L

The effect of NO_3^- to Fe(II) oxidation was also tried to be simulated in Phreeqc. After 60 minutes of simulation time, the NO_3^- concentration stayed constant, indicating no reaction of NO_3^- with other substances. Moreover, the differences in NO_3^- concentration did not make any difference to the simulated Fe(II) oxidation. This meant that the acceleration of Fe(II) oxidation by NO_3^- that was observed in the experiment was not achieved through a reaction between Fe(II) and NO_3^-.

Alas, it can be concluded from this experiment that the acceleration of Fe(II) oxidation by nitrate was related to pH. Nevertheless, further investigation is needed by keeping the pH during the oxidation experiment constant to eliminate the effect of pH on the oxidation to draw a more certain conclusion on the effect of nitrate on Fe(II) oxidation. Aside from that, no previous study was found that explain the effect of NO_3^- on Fe(II) oxidation in aerobic condition.

Aside from the effect of NO_3^- on Fe(II) oxidation, the effect on floc formation was also investigated. The effect of NO_3^- on floc formation and filtration is discussed further in chapter 4.2.1.

4.1.3. Effect of HCO_3^-

Alkalinity is the capacity of water to resist acidification and is usually in the form of bicarbonate in water samples with a pH <8.3 (Boyd, 2015). During oxidation and hydrolysis of iron, H^+ ions are released and can lower the pH of the water. The results from the effect of pH in section 4.1.1 showed that lower pH decreased the oxidation rate of Fe(II). Since alkalinity can resist acidification, the effect of bicarbonate on iron oxidation was investigated in this study.

The effect of bicarbonate on Fe(II) oxidation was studied by varying the concentration of bicarbonate from 1 mmol/L to 2 mmol/L. The result depicted in **Figure 4. 8** shows that a higher concentration of bicarbonate accelerated the oxidation of Fe(II). In solution with 1 mmol/L of bicarbonate, the concentration of Fe(II) was 0.02 mg/L after 30 minutes, whereas in solution with 2 mmol/L of bicarbonate, the concentration of Fe(II) was already 0.00 mg/L in 20 minutes. Simulation using Phreeqc also resulted in a higher oxidation rate with a higher bicarbonate concentration.

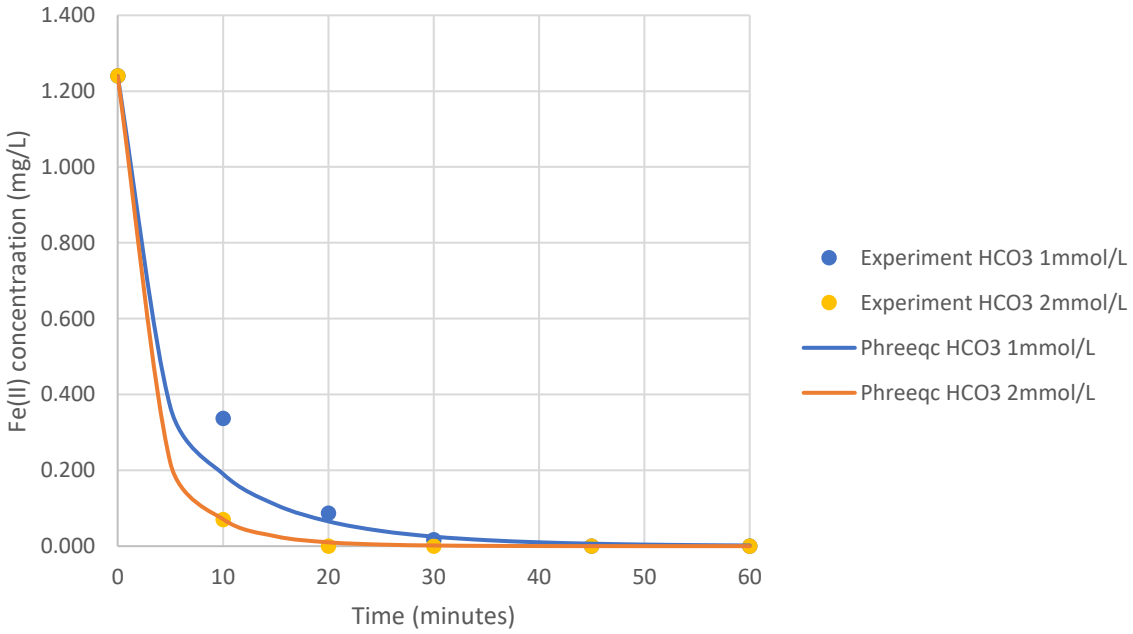

Figure 4. 8 Effect of bicarbonate on Fe(II) oxidation

The higher oxidation rate observed in solution with 2 mmol/L of bicarbonate was linked to the ability of bicarbonate to act as a pH buffer. As oxidation of Fe(II) occurred, the pH of the solution dropped and thus, the oxidation rate of Fe(II) became slower. However, higher bicarbonate concentration provided buffering capacity that presented an excessive drop of pH as can be seen in **Figure 4. 9**. In solution with 1 mmol/L of bicarbonate, the pH initially dropped to about 7.61 after 10 minutes, whereas in solution with 2 mmol/L of bicarbonate, the pH only dropped to 7.75. Thus, the ability of bicarbonate to keep the pH at a higher level can keep the oxidation rate to be maintained at a higher rate.

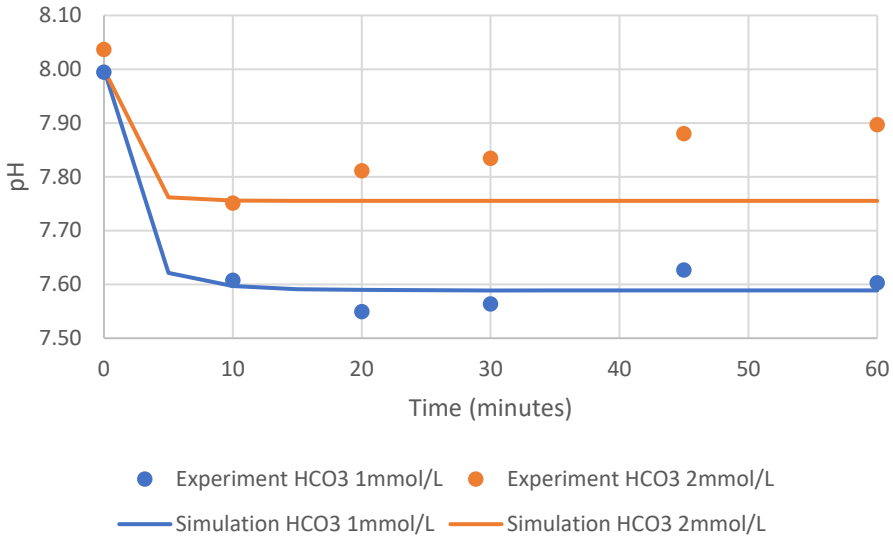

Figure 4. 9 Changes of pH during oxidation experiment and simulation at bicarbonate concentration of 1 mmol/L and 2 mmol/L

4.2. Column Experiment

Oxidation of Fe(II) and its subsequent hydrolysis produce iron flocs that can be removed through rapid sand filtration. The column experiment was conducted to study whether the flocs that were formed during oxidation could be retained by the sand filter.

4.2.1. Effect of nitrate on iron floc filtration

The first iron floc filtration experiment was done to investigate the effect of nitrate on the flocculation of iron and the filtration of iron. The experiment was done by oxidizing Fe(II) for 45 minutes in the solution at pH_{init} of 8 and nitrate concentration of 12 mg/L and 24 mg/L. The result of the iron floc filtration is shown in **Figure 4. 10**. It was found that the Fe(II) was fully oxidized into Fe(III) after 45 minutes, which was expected according to the result from the batch oxidation experiment in section 4.1.1.

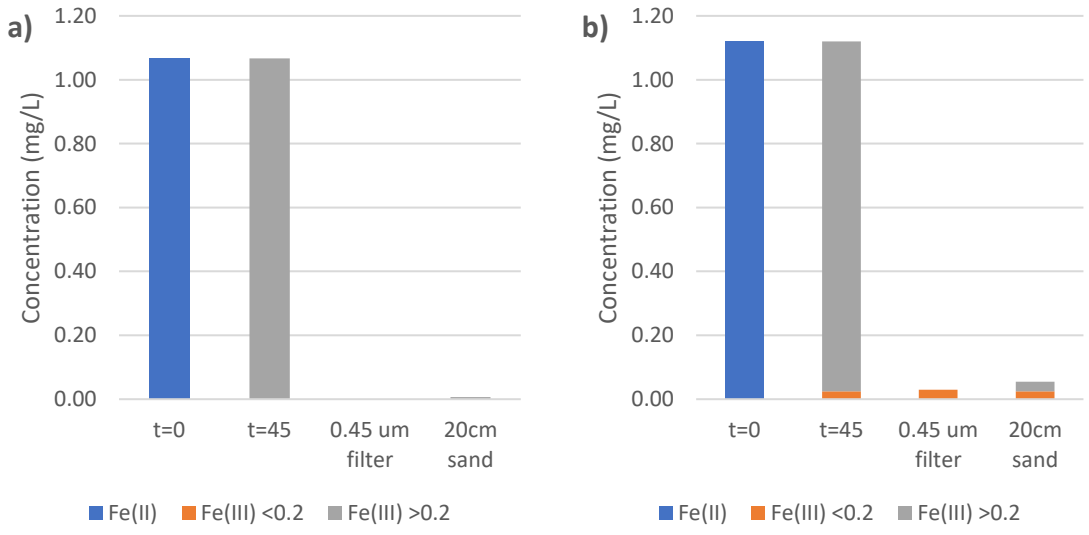

Figure 4. 10 The form of iron during oxidation at t=0 and t=45minutes and the result of filtration through 20 cm column filter of the solution containing nitrate at a concentration of (a) 12 mg/L (b) 24 mg/L

Although the iron was completely oxidized after 45 minutes, the sizes of the iron floc differed between the one in the solution containing 12 mg/L and 24 mg/L of nitrate. In the solution containing 12 mg/L of nitrate, the size of all of the Fe(III) floc was larger than 0.45 µm. In contrast, 3% (0.03 mg/L) of the iron floc in the solution containing 24 mg/L of nitrate passed through 0.2 µm and 0.45 µm filters.

After the Fe(II) was completely oxidized, the solution was then pumped into the column filter. The filtrate was then sampled twice, the first was filtered through a 0.2 µm filter, and the second was not filtered.

The filtrate of the solution with 12 mg/L nitrates contained 0.01 mg/L iron. As the flocs in the solution containing 12 mg/L nitrates were >0.45 um, and the filtrate did not contain <0.2 µm iron floc, the size of the iron that passed through the column should be >0.45 µm.

The filtrate of the solution with 24 mg/L nitrates contained 0.06 mg/L of iron. Of this 0.06 mg/L, 0.03 mg/L was <0.2 µm and 0.03 mg/L was >0.2 µm. As the filtrate from the 0.45 µm filter also contained 0.03 mg/L of iron, the portion of iron that passed through the column filter should also be >0.45 µm. This result shows that iron flocs that are <0.2 µm could not be retained by the column filter. Moreover, some of the iron flocs that are >0.45 µm still passed through the sand filter. However, the exact size of the flocs that are around 0.45 µm was not determined.

This experiment shows that the sand filter was able to efficiently remove iron flocs from the solution when the size of the flocs is >0.45 µm. It also seems that nitrate has only little influence on the flocculation of iron. Even at a higher nitrate concentration of 24 mg/L, the iron concentration in the filtrate of the column filter was 0.03 mg/L which fulfilled the target of <0.1 mg/L.

4.2.2. Iron removal through the sand column at initial pH of 7.4

Another experiment was done to study the iron removal when the pH_{init} for oxidation was set to 7.4. The initial Fe(II) concentration was set to 1.17 mg/L and the nitrate concentration was set to 24 mg/L. It was found that after 45 minutes, the concentration of Fe(II) was reduced to 0.23 mg/L. It was also found that 0.05 mg/L of the Fe(III) has a size of <0.2 µm which means that at lower pH, the higher nitrate concentration also hinders the flocculation of iron. The result of the experiment is shown in **Figure 4. 11**.

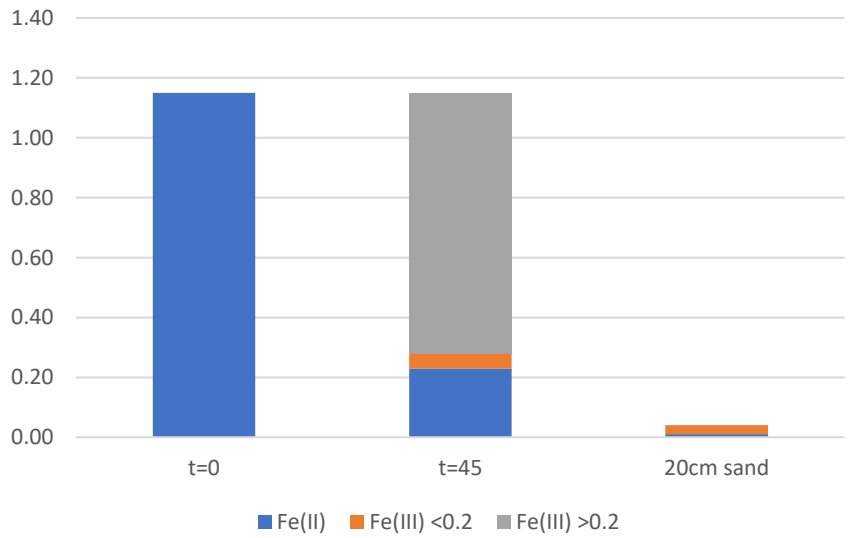

Figure 4. 11 Speciation of iron with pH_{init} of 7.4 before oxidation, after 45 minutes of oxidation, and after removal through the sand column

After filtering the water through the column, all of the Fe(III) that has the size of >0.2 µm was removed. In line with the result from filtration of flocs at pH_{init} of 8, there was Fe(III) that has a size of <0.2 µm that passed through the sand column. Moreover, the sand column was also able to remove Fe(II), as the concentration of Fe(II) in the filtrate was 0.01 mg/L. This means that aside from filtration of floc, the sand was also able to remove iron through adsorption of Fe(II).

4.2.3. Iron floc filtration breakthrough

For the iron floc filtration breakthrough experiment, the 20 cm sand was continuously fed with water containing iron floc. The experiment was conducted for 6 hours. The result is shown in **Figure 4. 12**. It was found that in the first 3 hours of filtration, the iron was completely removed by the column. Breakthrough of iron was observed after about 3.6 hours of filtration. The size of the iron that passed through the column at 3.9 hours, 5.2 hours, and 5.8 hours were >0.45 µm, whereas at 4.5 hours and 6.5 hours <0.45 µm iron flocs passed.

When the pores are clogged, the pore velocity increases, resulting in fewer flocs that can be retained. Due to the increase of pore velocity, shear force might also increase and exceed the shearing strength of the iron floc particles, breaking the flocs into a smaller size (Craft, 1966). This might be the reason why at 4.5 and 6.5 hours, <0.45 µm iron flocs passed the column filter. Nevertheless, the iron total concentration in the filtrate after breakthrough was far below the target of 0.1 mg/L.

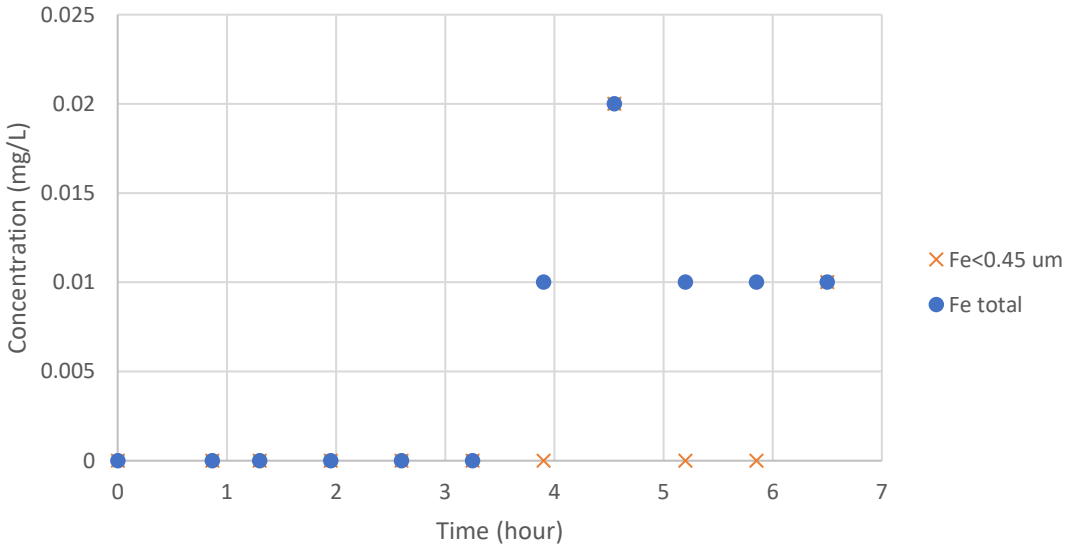

Figure 4. 12 The concentration of iron total in the filtrate of column filter over time during the 6.5 hours iron floc filtration breakthrough experiment

In addition to iron concentration, turbidity before and after filtration was also measured. The result is shown in **Figure 4. 13**. Excluding the outliers at 3.6 hours and 6 hours, the average turbidity before and after filtration was 1.75 NTU and 0.52 NTU respectively. The average turbidity removal before the iron breakthrough was 82%, whereas the average turbidity removal after iron breakthrough was 50%.

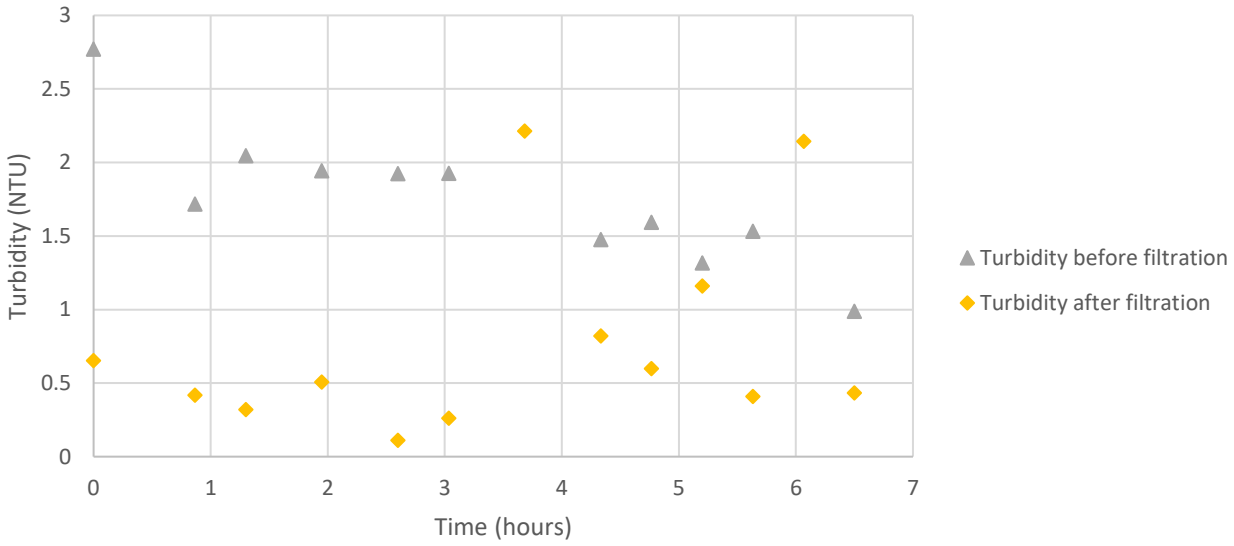

Figure 4. 13 The turbidity of the water before and after filtration during the breakthrough experiment

The breakthrough of either iron or turbidity can be used to estimate the time for backwashing. However, the breakthrough of iron through the 20 cm sand column cannot be translated directly to the breakthrough of full-scale rapid sand filtration. Nevertheless, estimation of the breakthrough in the full-scale rapid sand filter was attempted in this study.

The empty bed contact time (EBCT) of the column filter in this study was about 2.3 minutes. The EBCT of the sand filter in Emmen is roughly 16 minutes, which is around 6.9 times longer. By assuming the breakthrough of the small column at 3.4 – 3.5 hours and suppose the longer contact time can be used to estimate the breakthrough of the full-scale sand filter, the breakthrough time will be in the range of 23.6 – 24.3 hours for the full-scale sand filter.

It should be noted that removing iron through full floc filtration will result in rapid clogging and headloss of the rapid sand filter, necessitating more frequent backwash. In the treatment plant in Emmen, backwashing is done once a day (Hatenboer-Water, 2021).

4.2.4. Fe(II) adsorption breakthrough

The pH of the permeate in the treatment plant is in the range of 5.7 – 5.9 after RO membrane and between 6 – 7 after aeration. According to the oxidation experiment and modeling using Phreeqc, most of the iron will still be in the dissolved form of Fe(II) after 30 minutes in that pH range. Nevertheless, the treatment plant was able to remove the iron most of the time, and this led to the hypothesis that the sand filter removes the iron through adsorption. Furthermore, the hypothesis could not be rejected because the result from the iron removal experiment through the column at pH_{init} of 7.4 in section 4.2.2 showed a reduction of Fe(II) after sand filtration.

However, the sand has a certain capacity to adsorb Fe(II) and if the adsorbed Fe(II) is not oxidized, the breakthrough of Fe(II) can occur (Sharma, 2001). The iron breakthrough experiment through a 20 cm column was conducted to investigate when the breakthrough occurs. During the experiment, the initial concentration of the Fe(II) was 1.1 mg/L. The results are shown in **Figure 4. 14** and showed that the new sand that was used in the experiment can adsorb Fe(II). However, the breakthrough of Fe(II) was rather fast. After 30 minutes of filtration, 31% of the initial Fe(II) concentration was measured in the effluent. After 3 hours, 80% of the initial Fe(II) concentration was measured in the effluent.

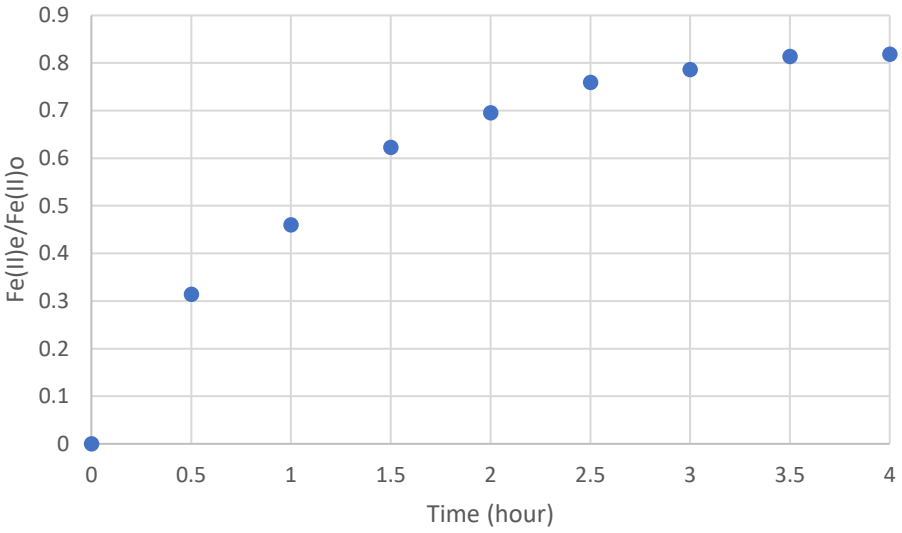

Figure 4. 14 Sand column filter Fe(II) adsorption breakthrough

Although the effect of pH was not investigated in this study, it has been previously found that higher pH increases the amount of Fe(II) that is adsorbed by sand (Sharma, 2001). This was due to the surface of the sand being more negatively charged with increasing pH, and consequently attracting more positively charged Fe(II) ions. In Sharma's experiment, a significant increase of isotherm constant of 400% is observed when the pH is increased from 6.0 to 7.5. This in turn also led to the longer breakthrough time of Fe(II) at a higher pH value (Sharma, 2001).

Compared to the study by Sharma (2001), the breakthrough curve observed in this study was less steep, as can be seen in **Appendix C**. This might be due to the water in this study was saturated with oxygen that allows oxidation of the adsorbed Fe(II). In Sharma's experiment, the water is anoxic as a result of deoxygenation by stripping with nitrogen gas, thus limiting the oxidation of the adsorbed Fe(II). The oxidized adsorbed Fe(II) also can adsorb another Fe(II), thus allowing more adsorption and prolonging the time of breakthrough. Moreover, the initial Fe(II) concentration that is used in Sharma's study is 4 mg/L, which is higher than the 1.1 mg/L that was used in this study. Aside from that, the sand that was used in this study might have a different adsorption capacity from Sharma.

This experiment was also limited to only using new sand as the media for the filter bed. Although an experiment using iron oxide coated sand was not carried out, it has been previously found that iron oxide coated sand has a higher Fe(II) adsorption capacity. Sharma (2001) found that iron oxide-coated sand can adsorb 5 times more Fe(II) compared to new sand, and the breakthrough took 5 times longer.

Furthermore, COMSOL was used to simulate the breakthrough of Fe(II) for the full-scale rapid sand filter. The description of the model and the underlying formulas are described in chapter **Error! Reference source not found.**. The values that were needed to be inputted were taken from a previous study on iron adsorption by Sharma (2001). When the values from Sharma were used, the model resulted in a faster adsorption breakthrough compared to the experiment. Thus, adjustment to adsorption parameters K_F, n, and k was made to fit the model to the experimental data.

The reference values for K_F, n, k, and D_L from Sharma (2001) are shown in **Table 3. 3**, and the final values that were inputted in COMSOL to fit the model are shown in **Table 4. 1**. Three parameters, namely K_F, n, and k, were adjusted by trial and error and the comparison with the reference values are shown in **Table 4. 2**. These three parameters were adjusted as they represent the adsorption isotherm and kinetics.

Table 4. 1 Final COMSOL model adjusted input parameters values

Parameters	Value	Description
k	2.3×10^{-4} /s	LDF kinetic rate coefficient
K_F	3.5×10^{-3} (mg/g)/(mg/m^3)^n	Freundlich isotherm constant
n	0.42	Freundlich empirical coefficient
D_L	1.6×10^{-4} m^2/s	Dispersion coefficient
c_0	0.02 mol/m^3	Fe(II) inflow concentration
ρ_b	1560 kg/m^3	Bulk density of sand
ρ_p	2600 kg/m^3	Particle density of sand
ε	0.4	Bed porosity
L	0.2 m	Column length
v	5.2 m/hour	Interstitial velocity

Table 4. 2 Comparison of the adjusted K_F, n, and k parameters with the reference values

	K_F [(mg/g)/(mg/m^3)^n]	n	K (s^{-1})
Reference values (Sharma, 2001)	0.0023	0.54	2.6×10^{-4}
Adjusted value	0.0035	0.42	2.3×10^{-4}

The predicted iron breakthrough curve for the 20cm filter is shown in **Figure 4. 15**. By adjusting the input values, the predicted model outcome was close to the experimental data. However, a slight difference was observed at adsorption time of 3 hours and beyond. The experimental data showed a gentler slope compared to the predicted model. This could be because the Fe(II) that was adsorbed to the sand particle was oxidized. Thus, more Fe(II) in the water can be adsorbed due to the availability of more Fe(III)hydroxide. In contrast, the COMSOL model was only able to simulate pure adsorption without oxidation of the adsorbed Fe(II).

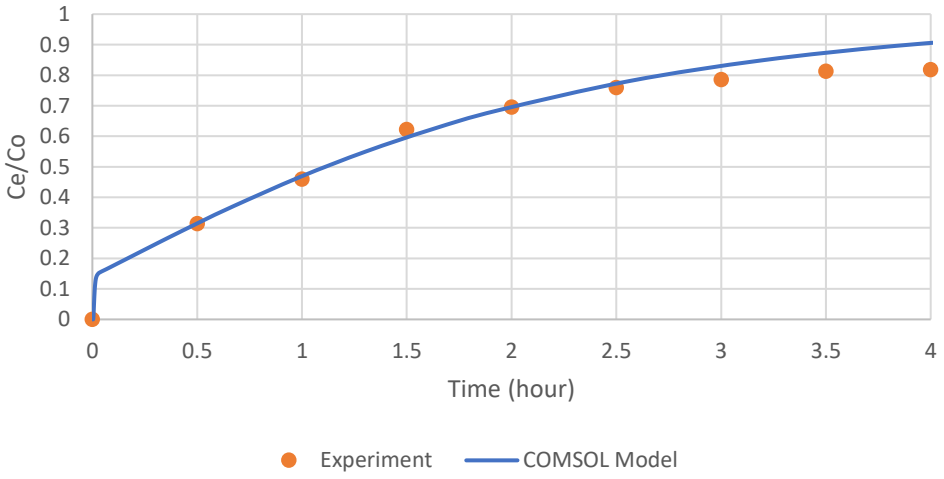

Figure 4. 15 Predicted and experimental iron breakthrough curves for 20cm filter column with new sand

Using the calibrated parameter values, the breakthrough for full-scale RSF was also simulated and shown in **Figure 4. 16**. As expected, a higher filter bed will result in a longer breakthrough time. The breakthrough of 10% iron was reached at 12.5 hours and 23.5 hours for 1.5 m and 2.6 m filters,

respectively. However, this result only predicts adsorption without the oxidation of adsorbed iron. With the oxidation of adsorbed iron, the breakthrough time should be longer.

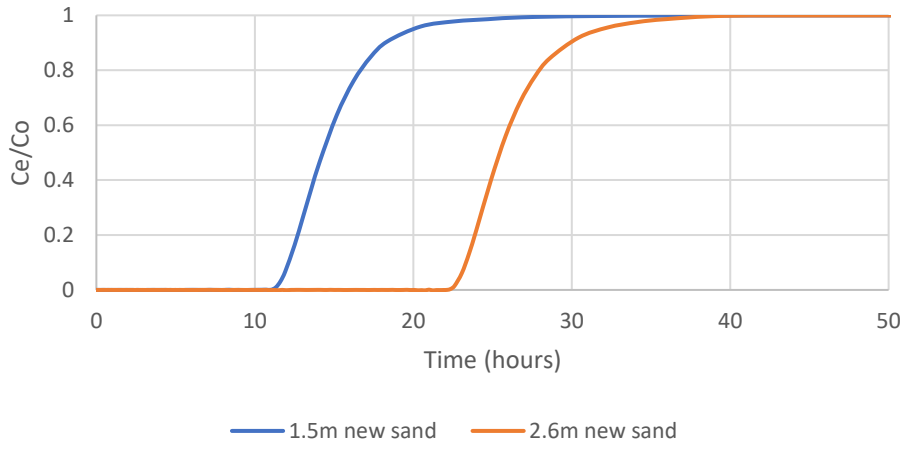

Figure 4. 16 Prediction of Fe(II) adsorption breakthrough for new sand filter with a bed depth of 1.5 m and 2.6 m

Prediction of Fe(II) adsorption breakthrough with iron oxide coated sand was also done using the values from Sharma (2001). The values were K_F = 42.7 x 10^{-3} (mg/g)/(mg/m^3)^n, n = 0.49, k = 1.7 x 10^{-4}/s, and D_L= 2.0 x 10^{-4} m^2/s (Sharma, 2001). For iron-coated sand, the breakthrough time will be longer because of the higher adsorption capacity of iron-coated sand as can be seen in **Figure 4. 17**. Aside from increasing sorption capacity, higher pH also accelerates the oxidation of adsorbed Fe(II). This can result in an even longer breakthrough time.

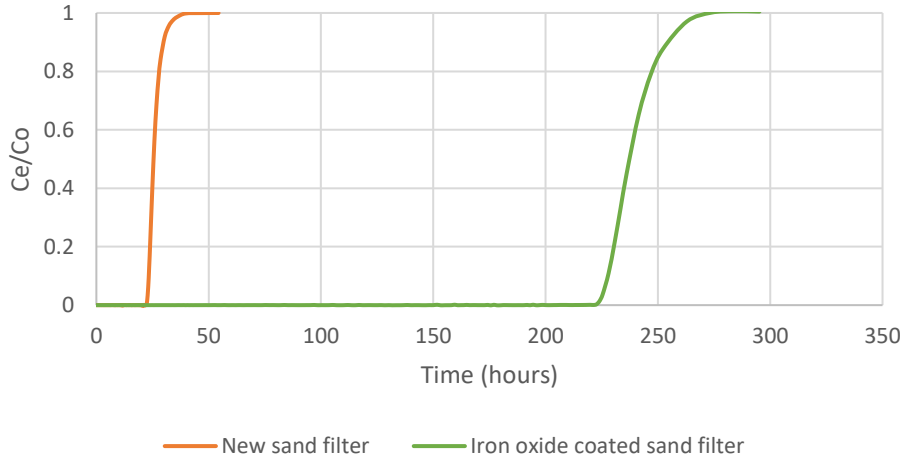

Figure 4. 17 Prediction of Fe(II) adsorption breakthrough for new sand filter and iron oxide-coated sand filter with a bed depth of 2.6 m

When breakthrough of iron occurs, the adsorption capacity must be regenerated by oxidizing the adsorbed Fe(II). This can be done by backwashing the filter using aerobic water to oxidize the adsorbed Fe(II) (Buamah et al., 2009). The efficiency of regeneration will depend on the duration of backwashing and the pH of the water that is used for backwashing. Backwashing with high pH water will oxidize the adsorbed Fe(II) rapidly.

In the treatment plant, the backwashing takes about 30 minutes. Currently, the filtrate of the sand filter is used to backwash the sand filter and has a pH in the range of 6.4 – 6.9. Based on the batch

oxidation experiment in chapter 4.2.1, only a small portion of the adsorbed Fe(II) would be oxidized within 30 minutes. Thus, complete adsorption site regeneration might not be achieved.

4.2.5. Sensitivity analysis of adsorption breakthrough modeling

The sensitivity of the breakthrough prediction for 2.6 m new sand to the change of parameter values was analyzed. The parameters that were analyzed were dispersion coefficient, kinetic rate, porosity, bulk density, and velocity. The values of the parameters were varied by ±30% of the values in **Table 4. 1**. The sensitivity analysis was done to assess how sensitive the model is to changes in the values of parameters (Murray-Smith, 2015). The results are shown in **Figure 4. 18**.

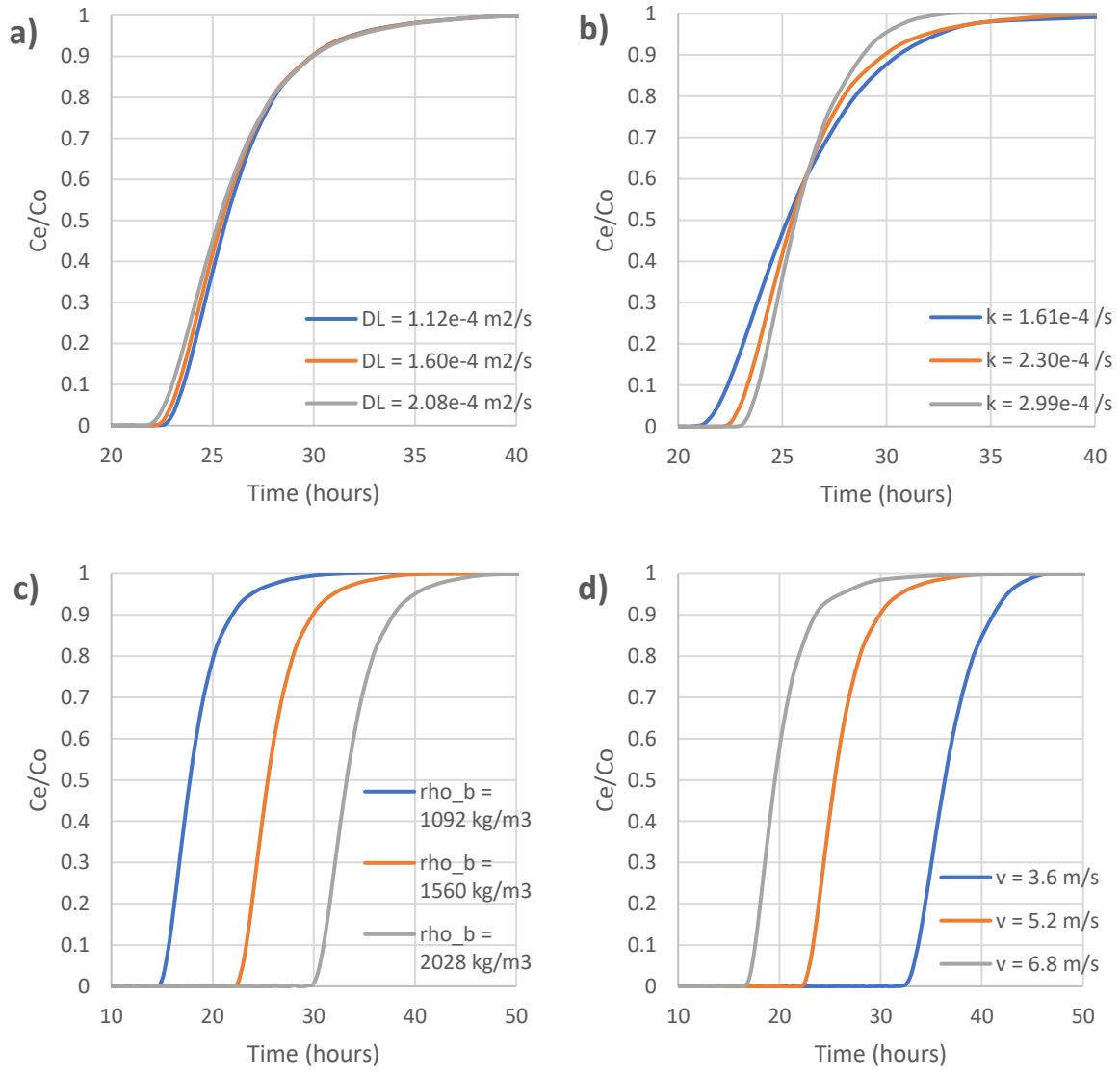

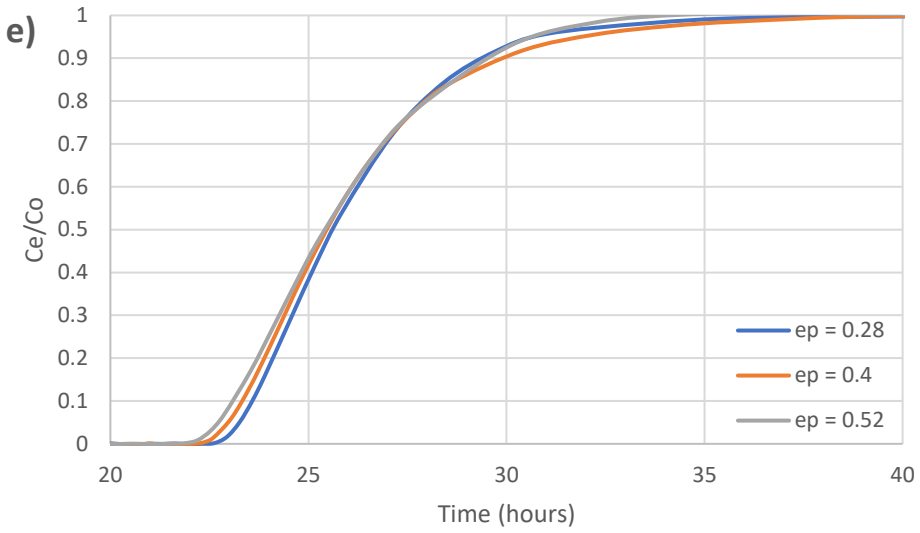

Figure 4. 18 Effect of **a)** dispersion coefficient, **b)** kinetic rate, **c)** bulk density, **d)** filtration velocity and **e)** porosity on the Fe(II) adsorption breakthrough prediction of 2.6 m new sand media

As can be seen from **Figure 4.18 c)** and **d)**, the model was very sensitive to bulk density and filtration velocity, thus an accurate measurement of these parameters is important to get an accurate prediction of the model. A 30% variation to the value of bulk density shifted the breakthrough about 7 hours. Filtration velocity also influenced the breakthrough greatly. A faster filtration velocity resulted in a faster adsorption breakthrough.

In addition, adsorption kinetics also somewhat influenced the adsorption breakthrough. Slower adsorption kinetics resulted in a faster breakthrough. Lastly, the porosity and dispersion coefficient seemed to have minimal impact on the adsorption breakthrough.

4.3. Analysis of the treatment plant

The treatment plant in Emmen is owned and operated by a farmer since 2016. The treatment plant is operated to produce water from March through October/November, following the cultivation and planting period of the farm. Throughout most of the time during the operation, the treatment plant can remove iron. However, it was reported by the farmer that the iron removal is sometimes not sufficient as iron passed the sand filter and ends up in the clear water tank. Even so, it is not known whether the iron floc passed through the sand filter or developed later in the clean water tank.

The farmer reported the problem in the frequency of once per year and even once per 2 years. One measurement was done on 13 May 2020 and found that the iron concentration in the effluent was 2.07 mg/L. In 2021, there has been no report from the farmer that the iron removal is not sufficient.

4.3.1. Iron concentration in the treatment plant

Measurement of iron concentration in the treatment plant has been done several times and can be seen in **Table 4. 3**. The iron concentration in the groundwater fluctuates. Measurement in March and May 2020 showed an iron concentration of >15 mg/L, whereas the iron concentration in March and April 2021 was <10 mg/L. The very low iron concentration found in April 2020 (0.67 mg/L) was probably due to a mistake in sampling or analysis.

Table 4. 3 Iron total concentration in the treatment plant in Emmen

Date		05/03/2020	20/04/2020	13/05/2020	17/06/2020	02/03/2021	15/04/2021
Fe-tot (mg/L)	Before RO	22.56	0.67	18.43	n/a	5.09	6.16
	After RO	1.28	10.6	1.79	n/a	n/a	1.14
	After Aerator	1.23	0.25	0.61	0.73	n/a	0.21
	After SF	n/a	0.01	2.07	0.011	0.04	0

Source: Hatenboer-water, 2020

It should also be noted that the concentration of Fe-total after aeration is less than the concentration before aeration. This could mean that iron removal is also happening inside the tower aerator. The iron removal in the tower aerator could be caused by oxidation of iron and precipitation on the packing material. This is indicated by the reddish deposits on the packing material as can be seen in **Figure 4. 19**.

Figure 4. 19 Packing material of the tower aerator

Aside from iron, the concentration of nitrate in the groundwater also varied (data shown in **Appendix D**). The concentration of nitrate was 149 mg/L, 19 mg/L, and 6.3 mg/L in March 2020, April 2020, and May 2020, respectively. The variation in nitrate concentration could be linked to the practice of fertilization in the agricultural area where the treatment plant is located. During the first planting period in March, more fertilizer was used compared to in April and May that might cause the higher nitrate concentration found in the source water in March.

4.3.2. Discussion about the tower aerator

Because the removal of iron is dependent on pH, the tower aerator is an important part of the system to strip CO_2 from the permeate and raise the pH of the permeate. The principle of CO_2 stripping is that the partial pressure of CO_2 in the air that comes in contact with water is less than the partial pressure of the CO_2 dissolved in the water, thus the dissolved CO_2 will be stripped off as a gas (Summerfelt et al., 2015). The CO_2 removal efficiency by the tower aerator will depend on air flowrate to water flowrate ratio (RQ) and contact time (Summerfelt et al., 2003). CO_2 stripping itself does not change the bicarbonate concentration and it was found that CO_2 stripping efficiency is independent of alkalinity (Summerfelt et al., 2015).

However, the pH of the permeate does not increase much after aeration. The pH of the permeate is in the range of 5.9 – 6.2. It was found that the pH after aeration increases to 6.4 – 7. There could be several reasons why the pH does not increase much:

- Iron oxidation and hydrolysis on the packing material releases H^+ that limits the increase of pH.
- Contact time between air and water is not sufficient to completely strip CO_2.
- Iron deposit on packing material clogs the aerator causing short-circuit flows and reduces airflow. The combination of short-circuiting and the lower airflow may reduce CO_2 stripping efficiency.

With the rise of pH as a result of CO_2 stripping, oxidation of Fe(II) also happens inside the tower aerator. According to van der Helm (1998), oxidation of Fe(II) in the tower aerator will generate CO_2 as described in the equation:

$$4Fe^{2+} + 8HCO_3^- + O_2 + 2H_2O \rightarrow 4Fe(OH)_3 + 8CO_2 \quad (4.1)$$

Due to the deposit of iron hydroxide on the packing materials, there will also be adsorption of Fe(II) and thus catalyzing the removal of iron in the tower aerator. According to van der Helm (1998), the oxidation and hydrolysis of iron in the tower aerator slightly reduce the CO_2 stripping efficiency by 2 – 4%. Simulation with Phreeqc was also conducted and resulted in a slightly lower CO_2 stripping efficiency at aeration duration of >180 seconds when Fe(II) oxidation happens as can be seen in **Table 4. 4**. At an aeration duration of <30 seconds, the CO_2 concentration and pH do not differ.

Table 4. 4 Comparison of pH and CO_2 concentration during aeration between with and without Fe(II) oxidation

Aeration duration (seconds)	CO_2 concentration (mg/L)		pH	
	No Fe(II) oxidation	Fe(II) oxidation	No Fe(II) oxidation	Fe(II) oxidation
0	152.91	152.91	5.90	5.90
10	119.31	119.31	6.01	6.01
20	93.13	93.13	6.12	6.12
30	72.75	72.75	6.22	6.22
180	2.66	2.71	7.66	7.65
300	1.05	1.31	8.06	7.96

Furthermore, the deposits (**Figure 4. 19**) can block and reduce airflow in the tower aerator. The lower RQ will impact the removal efficiency of not only CO_2 but also other gases such as H_2S and CH_4 from the water. At the same contact time, RQ 2 has 8 – 10% lower CO_2 removal efficiency compared to RQ 25 (**Table 4. 7**). In addition, clogging can cause uneven distribution of the water that flows inside the packed tower aerator. This can result in short-circuiting that reduces contact time between the air and water, and subsequently reduces the gas removal efficiency (Dyksen, 2012; TU Delft, 2004a).

The lower H_2S removal can be problematic because bisulfide can reductively dissolve Fe(III)hydroxides and release Fe(II) into the solution (Afonso & Stumm, 1992). The reaction mechanism can be described as follows (Yao & Millero, 1996):

(i) Surface complex formation

$$FeOH + HS^- \leftrightarrow FeS^- + H_2O \quad (4.2)$$

(ii) Electron transfer

$$FeS^- \leftrightarrow Fe^{II}S \quad (4.3)$$

(iii) Release of the oxidized product and detachment of Fe(II)

$$Fe^{II}S + H_2O \leftrightarrow Fe^{II}OH_2^+ + S^- \quad (4.4)$$

$$Fe^{II}OH_2^+ \rightarrow new\ surface\ site + Fe^{2+} \quad (4.5)$$

The reaction of H_2S with iron hydroxide involves the replacement of O^{2-} anions with S^{2-} and SH^-. Then, the highly reactive SH^- reacts with hydroxyl forms water and S^{2-}. Lastly, reduction of Fe^{3+} into Fe^{2+} is accompanied by oxidation of S^{2-} to elemental sulfur (Davydov et al., 1998).

In addition, the tower aerator is equipped with a reservoir. After aeration of the permeate, the iron can oxidize and flocculate in the reservoir. However, a pump is used to pump the water from the tower aerator to the rapid sand filter. The flocs that are already formed can be broken down when the water passes through the pump.

4.3.2.1. CO_2 concentration estimation

Because pH is an important factor that affects iron removal through either oxidation and floc filtration or adsorption, CO_2 stripping by the tower aerator is an important step to increase the pH of the permeate. To investigate the performance of the tower aerator in the treatment plant to strip CO_2, the concentration of CO_2 in the water needs to be estimated. The concentration of dissolved CO_2 was estimated using Phreeqc. The results of the CO_2 calculation are summarized in **Table 4. 5**.

Table 4. 5 Concentration of CO_2 in RO Feed, after RO, and after aeration with the corresponding pH and bicarbonate concentration

Units	pH	HCO_3 (mg/L)	$CO_{2\,(aq)}$ (mg/L)
RO Feed	6.8 - 7.1	189 - 244	27.5 - 66.8
After RO	5.9 - 6.2	37 - 67	61.1 - 167.0
After Aeration	6.4 - 7	43 - 55	8.6 - 43.70

The decrease of pH in the permeate compared to the influent stream was expected as the RO membrane rejects bicarbonate and shifted the bicarbonate equilibrium. In addition, percent recovery is a key design parameter of RO membrane, where the permeate flow for brackish water reverse osmosis is commonly operated at 75% – 85% of the feed flow (Alghoul et al., 2009; Tonner & Tonner, 2004). However, gases such as CO_2 pass through the RO membrane and are not rejected (Kneen et al., 1995). Therefore, the concentration of CO_2 in the permeate will be higher compared to the RO feed.

With aeration, CO_2 gas will be removed from the permeate and resulted in a lower CO_2 concentration compared to before aeration. However, the CO_2 cannot be stripped completely as the concentration of CO_2 present in the water will be in equilibrium with air (Gauntlett, 1980). The concentration of CO_2 in the permeate when in equilibrium with air was simulated using Phreeqc. The partial pressure of CO_2 in the air is about 400 ppm or 0.0004 atm. It was found that the pH of the permeate when in equilibrium with air will depend on the bicarbonate concentration as can be seen in **Table 4. 6**. The higher the bicarbonate concentration, the higher the pH can be.

Table 4. 6 The concentration of bicarbonate, the concentration of CO_2, and pH when CO_2 in the permeate is in equilibrium with air

HCO_3^- (mg/L)	CO_2 (aq) (mg/L)	pH
34.29	0.93	7.86
44.74	0.93	7.98
63.32	0.93	8.13

4.3.2.2. Tower Aerator CO_2 stripping efficiency

The theoretical efficiency of CO_2 stripping with counter-current flow can be estimated using the equation (van der Helm, 1998):

$$K = \frac{1 - e^{(-k_2.t(1-\frac{K_H}{RQ}))}}{1 - \frac{K_H}{RQ} e^{(-k_2.t(1-\frac{K_H}{RQ}))}} \quad (4.6)$$

The airflow of the tower aerator is 900 m^3/hour. With the flow rate of the water between 35 m^3/hour and 50 m^3/hour, the RQ of the aerator is between 18 – 25. Henry's law constant (K_H) for CO_2 is 1.23 at 10°C (TU Delft, 2004a). The k_2 was assumed to be 0.17/s (Gauntlett, 1980). With these values, the efficiency of stripping was calculated, and the results are shown in **Table 4. 7**. The calculation shows that higher contact time increases the CO_2 stripping efficiency. However, increasing the RQ from 25 to 100 did not increase the stripping efficiency much. Decreasing the RQ from 10 to 2 noticeably reduced the stripping efficiency.

Table 4. 7 Theoretical CO_2 stripping efficiency by counter-current tower aerator at RQ 2, 10, RQ 25, and RQ 100

Contact time (seconds)	CO_2 stripping efficiency (%)			
	RQ 2	RQ 10	RQ 25	RQ 100
5	50.14	55.81	56.68	57.11
10	70.59	79.69	80.93	81.53
20	87.53	95.53	96.24	96.56
30	94.09	99.00	99.25	99.36
60	99.23	99.99	99.99	100

Currently, the tower aerator can strip some CO_2 as can be seen in **Table 4. 5**, where the concentration of CO_2 after aeration is lower compared to before aeration. However, clogging of the packing material seems to have a negative impact on the CO_2 stripping efficiency. The stripping efficiency was higher after the packing material was replaced with a clean one. As can be seen in **Table 4. 8**, the stripping efficiency was <70% when the packing material was clogged, whereas after the packing material was replaced, the stripping efficiency increased to 86%. This could be because when the packing material was clogged with iron deposits, the airflow was reduced and short-circuiting happens that reduces stripping efficiency.

Nevertheless, CO_2 removal by packed tower aerators is intrinsically limited because at pH >7 the stripping becomes slower (Contreras, 2007; Lantec, 2013) and practically hard to achieve an increase of pH to >7 (Raschig, 2020).

Table 4. 8 Current CO_2 stripping efficiency by tower aerator

	Concentration of CO_2 (aq) (mg/L)		Stripping efficiency	Stripping efficiency needed to reach pH 7.9
	Before aeration	After aeration		
Before ring replacement	144.58	43.7	69.8 %	98.5 – 99.4%
After ring replacement	61.12	8.58	86.0 %	

4.3.2.3. Estimation of contact time in the tower aerator

The stripping efficiency after the replacement of packing material is still way below the efficiency that is needed to strip the CO_2 to reach equilibrium concentration with air. This could be because the contact time between the water and air is not enough. However, there are many uncertainties in estimating the contact time in the tower aerator.

The contact time was estimated by considering the velocity of the free-falling water droplet. Since the tower aerator contains packing material, water droplets would collide with the surface of the packing material. The drop impact behavior (deposition, rebound, and splash) depends on several parameters such as water impact velocity, surface tension, liquid viscosity, packing material surface roughness, hydrophobicity, and hardness (Chiang et al., 2017; Zhang et al., 2021).

Due to the collision, the splashed droplet will have lower potential energy and slower velocity compared to the free-falling water droplet (Chiang et al., 2017). By splashing on a wood surface, Chiang et al. (2017) found that the splashed droplet has 0.17% of the initial potential energy of the impacting droplet. Furthermore, the velocity of the droplet can also be slowed down by the air current that comes from below the aerator tower in a counter-current aeration.

The terminal velocity of the water droplet will depend on the diameter of the droplet. However, the water droplet needs to have a certain falling distance before reaching that terminal velocity (van Boxel, 1998). Thus, due to the uncertainty of the droplet velocity, velocity after splashing, and the effect of counter-current airflow, several assumptions were made.

It was assumed that the initial droplet velocity is 8 m/s. Assume the weight of the water droplet is 0.05 grams, the kinetic energy became 1.6×10^{-3} Joules. Assume the potential energy is equal to the kinetic energy and due to splashing, the potential energy is 0.5% of the initial potential energy and became 1.6×10^{-5} Joules.

Then, it was assumed that the new kinetic energy is the same as the new potential energy and the mass of the droplet stays the same. Thus, the new velocity became 0.56 m/s. Lastly, it was assumed that the airflow from below reduces the droplet velocity by half, thus the velocity of the droplet became 0.28 m/s.

With the height of the tower aerator at 3.6 m and the velocity of the droplet at 0.28 m/s, the contact time becomes 13 seconds.

By using equation 4.6, the CO_2 stripping efficiency with a contact time of 13 seconds is 88.30% for RQ 25 and 88.01% for RQ 18. The current CO_2 stripping efficiency of the tower aerator with clean packing materials is 86% (**Table 4. 8**), which is slightly lower than the efficiency calculated using the estimated contact time of 13 seconds.

Nevertheless, there are uncertainties regarding the contact time of the tower aerator and also the kinetic parameter of the gas transfer. Furthermore, as CO_2 is stripped, less free CO_2 is available to be stripped. Thus, the CO_2 transfer to the air becomes slower, and more residence time is needed to reach the theoretical CO_2 stripping efficiency (Lantec, 2013).

4.3.3. Retention time estimation of the tower aerator and the rapid sand filter

The calculation of retention time is needed to investigate whether the retention time in the aeration unit and rapid sand filtration is enough for iron oxidation and floc filtration. The contact time of the tower aerator was estimated in section 4.3.2.2 and resulted in a contact time of 13 seconds. Aside from that, the tower aerator is equipped with a reservoir as can be seen in **Figure 4. 20**. The volume of the reservoir was calculated to be 2.69 m^3. With a flow rate of 35 m^3/hour, the retention time in this reservoir was estimated to be about 4.6 minutes.

Figure 4. 20 Reservoir of tower aerator

Furthermore, the calculation of the retention time in the sand filter was divided into the retention time in the water above the sand filter and inside the filter bed. The sand filter is designed with a design velocity of 10 m/hour. The height of the water above the sand filter was assumed to be 1 m, thus the retention time above the sand filter is 6 minutes. The height of the filter bed is 2.6 m, thus the EBCT in the filter bed is 15.6 minutes. Assuming the porosity of the sand filter of 50%, the contact time in the bed became 7.8 minutes. Therefore, the total retention time in the sand filter is 13.8 minutes. Thus, the combined retention time of the tower aerator and the sand filter is 18.6 minutes.

Looking back at the result of the oxidation experiment in section 4.1, only 1.2% and 11.4% of Fe(II) were oxidized within 20 minutes for pH_{init} 6 and 7 respectively. Thus, the retention time of about <20 minutes in the treatment plant is not enough to achieve the removal of iron through floc formation and filtration. Since only a small portion of Fe(II) is oxidized, most of the iron is removed through adsorption.

4.4. Solution propositions

Iron removal in the water treatment plant happens through the combination of iron floc filtration and Fe(II) adsorption. The portion of which is more dominant will depend on different conditions. In a condition with high pH of 8, high oxygen concentration, low iron oxide concentration, and sufficient retention time before sand filtration, homogenous oxidation will be dominant, and the iron is removed dominantly by floc filtration. In the low pH range (6 – 7), high oxygen concentration, and high iron oxide concentration, adsorption of Fe(II) is dominant and will subsequently be followed by oxidation of the adsorbed Fe(II).

With a retention time of 18.6 minutes, iron removal that is dominated by iron floc filtration could not be achieved. At pH <7, most of the iron is still in the form of Fe(II) when the water enters the rapid sand filter. Even at pH_{init} of 8, 30 minutes was needed to fully oxidize and flocculate the iron. Therefore, adsorption of Fe(II) is the dominant mechanism of iron removal in the treatment plant. The similarity between iron floc filtration and Fe(II) adsorption is that both mechanisms are positively influenced by pH. Thus, increasing pH will improve iron removal.

4.4.1. Packing material cleaning to maintain RQ of the packed tower aerator

The deposit of iron on the packing material of the aeration tower can block the airflow and reduce the RQ. Lower RQ can reduce the stripping efficiency of gases from water. Aside from reducing RQ, the

deposits can create short-circuiting in the tower aerator and reduce the contact between water and air. Thus, periodical cleaning or replacement of the packing material is needed to keep the RQ high and prevent short-circuiting. Nevertheless, the ability of the packed tower aerator to strip CO_2 and increase pH is limited as discussed in chapter 4.3.2.2. Therefore, additional treatment to increase pH is still needed.

Currently, the packing materials of the tower aerator are replaced yearly. However, the build-up rate of deposits on the packing material is still not known. In addition, the RQ in the tower aerator when blocking happens is also not yet known. This information might be useful to determine when to replace the packing material. It is expected that replacing the packing material will cost 2,000 Euro. If replacement is done twice a year, the cost will be 4,000 Euro/year.

4.4.2. Improve CO_2 stripping to increase pH by installing another aerator

Since higher pH is preferable for iron removal and the current CO_2 stripping efficiency is still below the target stripping to reach a pH of 8, improving the CO_2 stripping is the first proposed solution. Calculation in section 4.3.2 showed that the contact time for the 3.6 m tower aerator of 13 seconds is not sufficient to completely remove CO_2. Thus, increasing the contact time to improve CO_2 stripping would be necessary.

To increase the contact time, a second aerator might need to be installed. However, the additional contact time that can be provided by another packed tower aerator is marginal. Therefore, another type of aerator that can provide a longer contact time might need to be employed such as an up-flow co-current bubble column reactor. The air bubble will pick up CO_2 from the water and vent it when the bubbles reach the water surface (Koweek et al., 2016). In this reactor, both the water flows co-currently to the flow of the air. The unit is illustrated in **Figure 4. 21**.

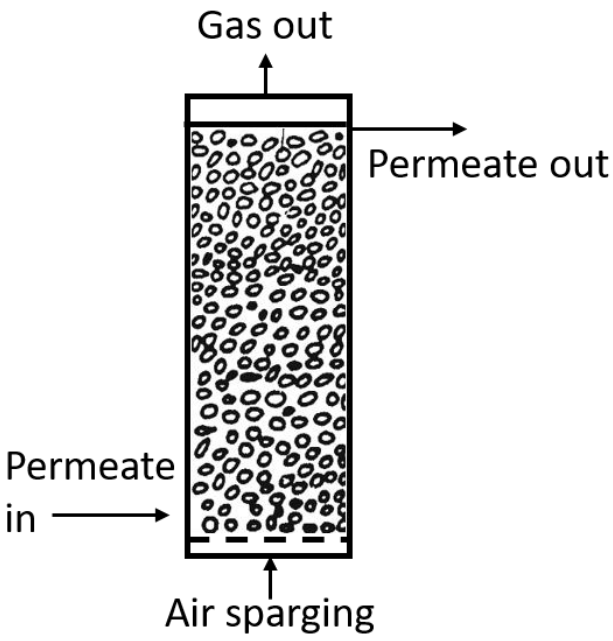

Figure 4. 21 Illustration of an up-flow bubble column reactor (Jakobsen, 2014b)

Position of the bubble column reactor in the treatment train

The co-current upflow bubble column reactor can be put before the packed tower aerator to avoid using a pump by taking advantage of the available pressure of 1.5 bar after the RO membrane. However, the permeate was expected to contain H_2S gas aside from CO_2. The H_2S is more soluble than CO_2 and thus

will be harder to strip compared to CO_2 (Lochrane, 1977). The removal of H_2S is best at low pH because the H_2S will dissociate into bisulfide (HS^-) at higher pH (Duranceau et al., 2010).

Since CO_2 is more readily strippable, the pH was expected to increase fast and the H_2S is dissociated into HS^-. The HS^- itself cannot be removed by the subsequent packed-tower aerator because it cannot be removed as gas at a higher pH. Thus, the higher pH reduces the efficiency of H_2S removal. In addition, because HS^- is present, the iron removal can be potentially hindered as described by equation 4.2 – 4.5.

Nevertheless, the concentration of H_2S in the permeate is not known. Therefore, further study is needed to determine the concentration of H_2S and its effect on iron oxidation and hydrolysis in the bubble column reactor. If the concentration of H_2S does not significantly hinder the removal of iron and the bubble column reactor can remove CO_2 efficiently, the packed tower aerator can be redundant and replaced entirely by the bubble column reactor.

In addition, Fe(II) is also oxidized in the bubble column reactor. If the bubble column reactor is placed before the packed tower aerator, the Fe(III) precipitate can clog the packing material. Nevertheless, it is still uncertain whether the build-up of deposits will be faster or not. If the deposit build-up is faster, the regular cleaning/replacement of the packing material will be more frequent and the maintenance cost will be higher. In addition, the water still needs to be pumped from the packed tower aerator to the rapid sand filter. The flocs that have already formed might break and might pass the rapid sand filter.

Therefore, the bubble column reactor was proposed to be put after the packed tower aerator. It should be noted that the outlet of the bubble column reactor should be higher than the rapid sand filter to avoid pumping.

Basic theory for dimensioning the bubble column reactor

The stripping of CO_2 in a bubble column reactor could be determined by the mass transfer coefficient on the liquid side (k_L), gas-liquid interfacial area (a), and the CO_2 concentration gradient between the water and in the film bubble interface (Huber, 2011).

The mass transfer coefficient on the liquid side (k_L) does not depend on aeration conditions and can be considered constant. The typical k_L value for CO_2 in bubble columns is between 10^{-4} – 10^{-5} $m.s^{-1}$ (Huber, 2011). The variation of volumetric mass transfer coefficient values is influenced by the interfacial area. Thus, knowing the value of the interfacial area (a) is essential for designing bubble column reactors (Jasim, 2016). The value of *kLa* is formulated as (Tirunehe & Norddahl, 2016):

$$k_L a\ (s^{-1}) = k_L\ \left(\frac{m}{s}\right).a\ \left(\frac{m^2}{m^3}\right) \tag{4.7}$$

The interfacial area itself is dependent on the diameter of the bubble in the bubble column reactor. A larger bubble will have a smaller exchange area (Hernandez-Alvarado et al., 2017; Tirunehe & Norddahl, 2016). The average bubble diameter of conventional bubble columns is ~5 mm and the interfacial area is 200 – 300 m^2/m^3 (Bouaifi et al., 2001). A higher interfacial area of 1000 – 4500 m^2/m^3 can be attained by using microbubble dispersion generators to generate smaller bubbles (Hernandez-Alvarado et al., 2017).

Required contact time estimation to increase pH to 8

To estimate the contact time needed for CO_2 stripping to achieve an increase of pH to 8, Phreeqc was used, and the code is shown in **Appendix F**. The CO_2 stripping rate can be described by the liquid mass balance for total dissolved inorganic carbon (Huber, 2011):

$$\frac{d[DIC]}{dt} = k_L a([CO_2] - [CO_2 equilibrium]) \quad (4.8)$$

It was assumed that the k_L value is 5 x 10^{-5} m.s^{-1} and the interfacial area is 500 m^2/m^3. These values generated a *kLa* of 0.025/s.

The bubble column reactor was used to supplement the CO_2 stripping by the packed tower aerator. Thus, the characteristic of the permeate after packed tower aerator was used as an input for Phreeqc. The pH_{init} was set at 6.2, and the bicarbonate concentration was 50 mg/L. The equilibrium concentration of CO_2 was assumed to be 0.93 mg/L as calculated in **Table 4. 6**. The Fe(II) after the packed tower aerator was assumed to be 0.67 mg/L. As pH increases, the oxidation of Fe(II) becomes faster and hindered the increase of pH by CO_2 stripping. The result of the CO_2 stripping model with the influence of Fe(II) oxidation is shown in **Figure 4. 22**.

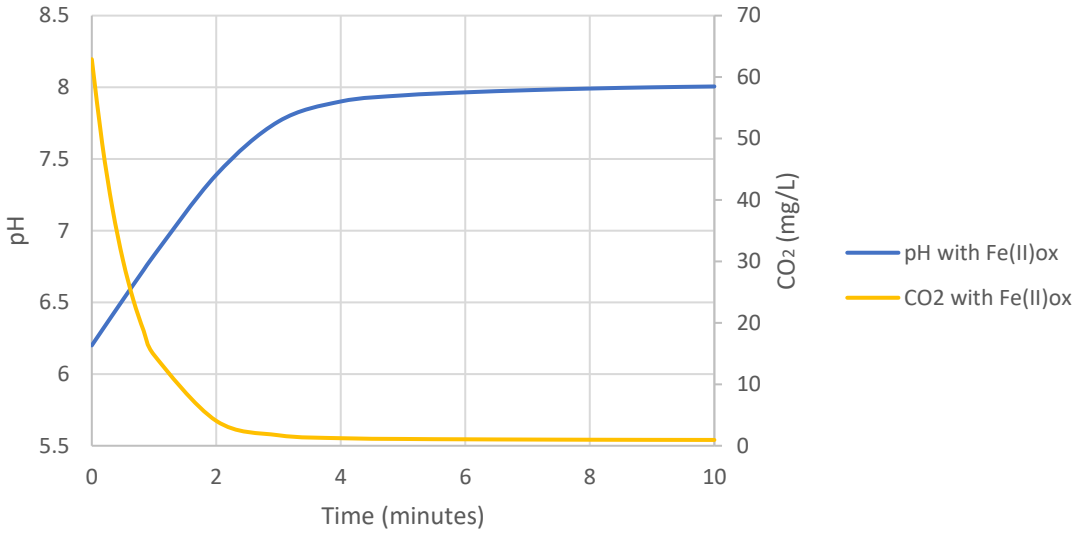

Figure 4. 22 Predicted changes of pH and CO_2 concentration as a result of CO_2 stripping by bubble column reactor

As can be seen in **Figure 4. 22**, the contact time that is needed to reach pH 8 was 7 minutes with the influence of Fe(II). The CO_2 stripping and the increase of pH were rapid in the first 3.5 minutes. However, the increase became marginal after reaching pH 7.9 at 4 minutes. Because the pH 7.9 is close enough to the target pH of 8 and already sufficient for iron removal, the retention time of 4 minutes was used to design the bubble column reactor.

In addition, another simulation was also conducted with an initial CO_2 concentration of 153 mg/L and pH_{init} of 5.9 to simulate the omission of the packed tower aerator. With the aforementioned condition, 5 minutes were needed to increase the pH to 7.9 which is 1 minute longer compared to when the packed tower aerator is still used. In 5 minutes, the CO_2 concentration decreased from 153 mg/L to 1.3 mg/L.

The evolution of Fe(II) concentration due to oxidation in the bubble column reactor is shown in **Figure 4. 23**. In the beginning, the oxidation of Fe(II) was slow because the pH of the water was still low. The oxidation became rapid after 2 minutes when the pH reached 7.4. After 7 minutes of aeration, the Fe(II) concentration was decreased from 0.67 mg/L to 0.13 mg/L. After 9 minutes of aeration, the Fe(II) concentration was <0.1 mg/L.

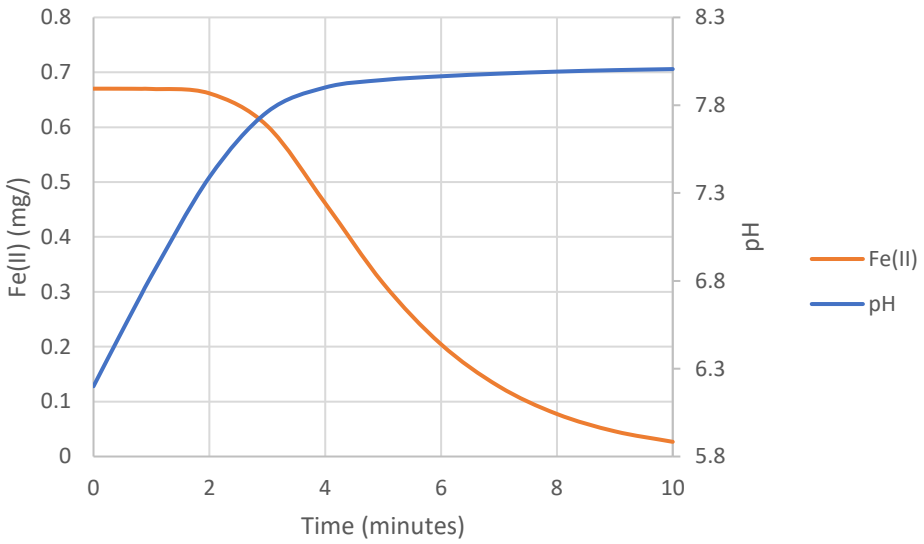

Figure 4. 23 Predicted changes of Fe(II) concentration and pH as a result of CO_2 stripping by bubble column reactor

Dimension of the bubble column reactor

It was assumed that the height of the bubble column reactor is 3 m. For a water flow rate of 35 m^3/hour and retention time of 4 minutes, the required volume is 2.3 m^3. Thus, the diameter of the column is 1 m. Therefore, the height-to-diameter ratio is 3. As a comparison, bubble column reactors that are used for biochemical applications have a length-to-diameter ratio of 2 – 5 (Kantarci et al., 2005). A larger diameter is usually desirable to provide larger gas throughputs and a higher column is necessary for large chemical conversion levels (Krishna et al., 1997).

Airflow rate requirement

For a bubble column reactor that is operated in a continuous system, the liquid superficial velocity should be maintained to be lower than the gas superficial velocity by at least 10x (Kantarci et al., 2005). With a column height of 3 m and retention time of 4 minutes, the liquid velocity is 1.25 cm/s. Thus, the bubble column reactor should be operated with a superficial gas velocity of at least 13 cm/s. The superficial gas velocity is expressed as the volumetric flow rate divided by the cross-sectional area of the column (Kantarci et al., 2005). Thus, the minimum required volumetric flow rate of the air is 350 m^3/hour for a water flowrate of 35 m^3/hour. A higher airflow rate can increase the efficiency of CO_2 stripping and higher pH can be achieved (Contreras, 2007).

Cost estimation

It was assumed that the capital cost of bubble column reactors is 2,000 Euro/m^3 (Humbird et al., 2017). The volume needed for the water in the bubble column reactor was 2.3 m^3. Thus, the CAPEX for the bubble column reactor is 4,600 Euro.

The operational cost of the bubble column reactor was contributed by the operation of the blower. It was assumed that to supply 500 m^3/h of air, the required power is 6 kW (HR Blowers, 2021). The bubble column reactor was expected to be operated for 9 months or 270 days per year. Thus, the power consumption per year is 38,880 kWh. It was assumed that the energy price is 0.1 Euro/kWh. Thus, the OPEX was 3,900 Euro/year.

If the existing blower for the packed tower aerator can be modified to also supply air for the bubble column aerator, no additional blower will be needed. In addition, if the packed tower aerator can

be replaced completely by the bubble column reactor, the existing blower can be repurposed for the bubble column reactor. Thus, there will be no additional OPEX. Furthermore, because the bubble column reactor contains no moving parts and is not susceptible to clogging, the maintenance cost would be low.

Additional note and disclaimer

Nevertheless, it should be noted that the modeling was simplified. In reality, the hydrodynamics of bubble column reactors is more complex. The flow of the bubbles may not be homogeneous as bubbles can coalesce to form larger bubbles. The large bubbles can rise faster than the smaller bubbles (Jakobsen, 2014a). In addition, larger bubbles have a smaller interfacial area and lower *kLa* value that may reduce the transfer of gases from the water to the bubbles.

In addition, the author could not find any information regarding the minimum concentration of H_2S that can hinder iron removal in previous literature. Thus, it was assumed that the concentration of H_2S in the permeate is negligible, even though it can fluctuate in the field.

Furthermore, the model could not be validated as an experiment was not done. Although the modeling resulted in sufficient CO_2 removal, the author is still not sure whether the bubble column reactor can work to efficiently remove CO_2 and increase pH without an experimental result at lab scale or pilot scale to validate the model. Further experimental study or more complex modeling might be needed to confirm whether the bubble column reactor can remove CO_2 and H_2S efficiently or not.

4.4.3. Provide detention tank after the tower aerator to allow longer time for iron oxidation and flocculation

The tower aerator is equipped with a reservoir, and flocculation of iron can happen in the reservoir. However, the water from the reservoir is pumped to the rapid sand filter. The turbulence that happens in the pump can break the flocs into smaller sizes (van der Helm, 1998). The idea behind this solution is to provide some time to allow the flocs to form a bigger size again. The tank should be located above the rapid sand filter to allow the flow of water to the rapid sand filter without a pump.

However, the addition of a detention tank will not increase the pH of the water. In the long run, the adsorption capacity of the sand filter might get exhausted if the pH is not increased. For a water flow rate of 35 m^3/hour and an additional detention time of 10 minutes, the required volume of the detention tank is 6 m^3.

It was assumed that the price of tanks is 100 Euro/m^3. Thus, the CAPEX for the detention tank is 600 Euro.

4.4.4. Alkaline dosing after aeration to increase pH

If tweaking the tower aerator is not enough to increase the pH of the water to 8, base dosing can be done to increase the pH. The dosing should be done after the aeration. The dose depends on the pH of the water after aeration. NaOH is a base that is commonly used to increase the pH of water. However, excessive Na can be toxic to plants because it contributes to salinity problems, interferes with magnesium and calcium availability, and causes foliar burns (De Pascale et al., 2013).

Thus, a more preferable base that can be dosed is KOH since potassium is also a nutrient for plant growth. For the permeate with a pH of 6.4, the KOH dosing that is needed to reach pH 8 based on Phreeqc calculation was 1.1 mmol KOH/L of permeate. For the permeate with a pH of 7, the needed dose was 0.29 mmol KOH/L of permeate.

It should be noted that dosing KOH will increase the operational cost of the treatment plant. The requirement for KOH was calculated to be 4 ton – 14 ton/year. It was assumed that the price of KOH is 750 Euro/ton. Thus, the OPEX was estimated to be 3,000 – 10,500 Euro/year.

4.5. Overview of the solutions

Periodic replacement of packing material in the tower aerator is necessary to avoid clogging of the tower aerator. However, the CO_2 stripping by the tower aerator is intrinsically limited and the pH of the water after aeration was still 7 at maximum. Thus, the bubble column reactor will still be required to strip the CO_2.

Since the iron flocs might be broken by the pump after the packed tower aerator, a detention tank might be needed to allow the flocs to form a bigger size. However, it should be noted that there is a supernatant water level on top of the rapid sand filter. The detention tank might not be needed if the flocs can form a bigger size in this layer of water. Furthermore, the positioning of the bubble column aerator after the packed tower aerator might also negate the necessity of the detention tank.

The bubble column reactor was predicted to be able to increase the pH of the water to 7.9 based on the assumptions made in this study. Moreover, the bubble column reactor will provide additional retention time for Fe(II) oxidation. It was assumed that the up-flow velocity is higher than the settling velocity of iron flocs, thus the flocs will leave the reactor and not be deposited in the reactor. Moreover, the bubble column reactor does not contain moving parts aside from the blower. Therefore, it will require low maintenance.

In addition, the bubble column reactor can make the packed tower aerator redundant if the concentration of H_2S is low and the iron removal is not hindered. If the packed tower aerator is obsolete, the existing blower can be used to supply air for the bubble column reactor. Further cost-saving can also be obtained since cleaning and replacing the packing materials are no longer necessary. However, further study is needed to determine whether this is possible or not.

From the point of view of OPEX, periodic replacement of packing material and the operation of bubble column reactor is similar. Periodic replacement of packing material requires 4,000 Euro/year if replacement is done twice per year. For the bubble column reactor, the OPEX depends on the power of the blower. It was estimated that for a 6 kW blower, the annual OPEX for a bubble column reactor is approximately 3,900 Euro/year. For the same OPEX, the bubble column reactor is more beneficial as it can provide more detention time and increase pH to 7.9 which cannot be provided by periodic replacement of packing material. Additionally, there should be no additional OPEX if the bubble column reactor can replace the packed tower aerator entirely as the existing blower can be repurposed for the bubble column reactor.

The dosing of alkali would be the least preferable option. Dosing KOH might increase the pH and the potassium is beneficial for plants. However, the plants have a certain requirement for nutrients. Overdosing of chemicals can be disastrous to the plants. Since the dosing is dependent on the pH of the water, measurement of pH is necessary at all times to prevent overdosing or underdosing. Furthermore, dosing alkali would be costlier compared to periodic packing material replacement and bubble column reactor installation.

Final remarks

From all of the proposed solutions, it is strongly advised to install the bubble column reactor as it can strip CO_2 efficiently within the provided residence time of 4 minutes, increase pH to 7.9, and require low maintenance.

5
Conclusions and Recommendations

The purpose of this study was to investigate the iron removal problem in a water treatment plant in Emmen and propose a solution to improve iron removal. Conclusions and recommendations were drawn from the study as follows:

5.1. Conclusions

The farmer that owns the brackish groundwater treatment plant in Emmen reports insufficient iron removal from the treatment plant once per one to two years. Prior to this study, the cause of the iron removal insufficiency is still unclear. Batch iron oxidation experiment, column sand filtration experiment, and analysis of the treatment plant were conducted to investigate the cause of iron removal efficiency. The conclusions from the investigation are as follows:

1. **Is the retention time of the tower aerator and the sand filter sufficient to provide duration for fully oxidizing Fe(II) and flocculating the Fe(III)?**
   The combined retention time of the tower aerator and the sand filtration of 18.6 minutes is not sufficient to remove iron through floc filtration. At pH of the permeate between 6 – 7, only <11.5% of the initial Fe(II) was oxidized in 20 minutes.
2. **Does changing the pH of the permeate affect the oxidation rate of Fe(II) into Fe(III) and hinders the formation of the flocs to a size of <0.2 µm?**
   Increasing the pH of the permeate accelerates the oxidation of Fe(II) and subsequently, more iron hydroxide flocs are produced. The size of the flocs does not seem to be affected as most of the flocs have a size of >0.2 µm.
3. **To what extent does the concentration of nitrate in the permeate affect the oxidation rate of Fe(II) into Fe(III) and hinders the formation of the iron flocs to a size of <0.2 µm?**
   The nitrate within the concentration range that was investigated in this study significantly affects the oxidation rate of Fe(II) although different is not much. Nevertheless, it only has little and insignificant influence on the size of the formed iron flocs.
4. **Can the rapid sand filter retain the iron flocs that are formed after Fe(II) oxidation and hydrolysis, and also adsorb Fe(II)?**
   The rapid sand filter can retain the formed iron flocs. In addition, the sand filter is also able to adsorb Fe(II).
5. **What are the options to increase pH to >7 to improve iron removal?**
   A pH of approximately 8 is preferable to improve iron removal because it accelerates Fe(II) oxidation, and increases the capacity of filter media to adsorb Fe(II). The current CO_2 stripping efficiency by the tower aerator is not enough to increase the pH to >7. The tower aerator cannot completely strip CO_2 from the permeate due to insufficient contact time and clogging by deposits on the packing material. Increasing pH can be achieved by improving CO_2 stripping or dosing KOH. From these two options, improving the CO_2 stripping to increase the pH of the permeate is preferable. This can be done by installing a bubble column reactor.

5.2. Recommendations

To improve the operation of the treatment plant and improve the iron removal, several measures are recommended:

1. Daily measurement of pH in the permeate after RO and after aeration to monitor the performance of aerator to remove CO_2 and increase pH. Periodical measurement of pH is important to monitor the performance of the tower aerator. When the increase of pH is small, it indicates the time to clean or replace the packing material of the tower aerator.
2. Once per 2 days measurement of iron in the effluent of the sand filter using a simple colorimetric iron test kit, preferably that has a measuring range of 0.05 – 1.0 mg/L. Additionally, also measure the concentration of iron in the permeate after RO and after aeration using a more accurate method in monthly basis and when the colorimetric iron test kit indicates a concentration of >0.1 mg/L. The more measurement should discern between Fe(II) and Fe(III). It is important to measure the Fe(II) because it cannot be determined visually (dissolved Fe(II) is clear, not yellowish as Fe(III)).
3. Before implementing the bubble column reactor, it is best to conduct a pilot study to determine in the field whether the bubble column reactor can efficiently remove CO_2 and increase pH to 7.9. This is important to decide whether the bubble column reactor can completely replace the existing packed tower aerator.

Bibliography

Afonso, M. dos S., & Stumm, W. (1992). Reductive Dissolution of Iron(III) (Hydr)oxides by Hydrogen Sulfide. *Langmuir*, *8*(6), 1671–1675. https://doi.org/10.1021/la00042a030

Alghoul, M. A., Poovanaesvaran, P., Sopian, K., & Sulaiman, M. Y. (2009). Review of brackish water reverse osmosis (BWRO) system designs. *Renewable and Sustainable Energy Reviews*, *13*(9), 2661–2667. https://doi.org/10.1016/j.rser.2009.03.013

Bernardes, A. M. (2016). Conventional Pretreatment of Water. In E. Drioli & L. Giorno (Eds.), *Encyclopedia of Membranes* (pp. 459–462). Springer Berlin Heidelberg. https://doi.org/10.1007/978-3-662-44324-8_2087

Bohdziewicz, J., Bodzek, M., & Wąsik, E. (1999). The application of reverse osmosis and nanofiltration to the removal of nitrates from groundwater. *Desalination*, *121*(2), 139–147. https://doi.org/10.1016/S0011-9164(99)00015-6

Bouaifi, M., Hebrard, G., Bastoul, D., & Roustan, M. (2001). A comparative study of gas hold-up, bubble size, interfacial area and mass transfer coefficients in stirred gas-liquid reactors and bubble columns. *Chemical Engineering and Processing*, *40*(2), 97–111. https://doi.org/10.1016/S0255-2701(00)00129-X

Boyd, C. E. (2015). pH, Carbon Dioxide, and Alkalinity. In *Water Quality: An Introduction* (pp. 153–178). Springer International Publishing. https://doi.org/10.1007/978-3-319-17446-4_8

Buamah, R., Petrusevski, B., & Schippers, J. C. (2009). Oxidation of adsorbed ferrous iron: Kinetics and influence of process conditions. *Water Science and Technology*, *60*(9), 2353–2363. https://doi.org/10.2166/wst.2009.597

Chiang, C. Y., Yang, T. Y., Casandra, A., & Lin, S. Y. (2017). A study of the splash phenomenon of water drops on wood – Emitted droplet velocity and kinetic energy. *Experimental Thermal and Fluid Science*, *88*, 444–449. https://doi.org/10.1016/j.expthermflusci.2017.06.019

Contreras, E. M. (2007). Carbon dioxide stripping in bubbled columns. *Industrial and Engineering Chemistry Research*, *46*(19), 6332–6337. https://doi.org/10.1021/ie061350i

Craft, T. F. (1966). Review of Rapid Sand Filtration Theory. In *Journal - American Water Works Association* (Vol. 58, Issue 4). https://doi.org/10.1002/j.1551-8833.1966.tb01600.x

Cromphout, J., Lagast, H., Peleman, G., & Verdickt, L. (2013). Flotation outperforms sedimentation and ultrafiltration for turbidity and NOM removal at the drinking water treatment plant of Kluizen. *Water Science and Technology: Water Supply*, *13*(2), 302–308. https://doi.org/10.2166/ws.2013.023

Dart, F. J., & Foley, P. D. (1970). Preventing Iron Deposition With Sodium Silicate. In *Journal / American Water Works Association* (Vol. 62, Issue 10). https://doi.org/10.1002/j.1551-8833.1970.tb03987.x

Davydov, A., Chuang, K. T., & Sanger, A. R. (1998). Mechanism of H2S oxidation by ferric oxide and hydroxide surfaces. *Journal of Physical Chemistry B*, *102*(24), 4745–4752. https://doi.org/10.1021/jp980361p

De Pascale, S., Pardossi, A., & Orsini, F. (2013). Irrigation water quality for greenhouse horticulture. *Good Agricultural Practices for Greenhouse Vegetable Crops*, *January*, 169–204.

Domagalski, J. L., & Johnson, H. M. (2011). Subsurface transport of orthophosphate in five agricultural

watersheds, USA. *Journal of Hydrology*, *409*(1–2), 157–171. https://doi.org/10.1016/j.jhydrol.2011.08.014

Duranceau, S. J., Trupiano, V. M., Lowenstine, M., Whidden, S., & Hopp, J. (2010). Innovative Hydrogen Sulfide Treatment Methods : Moving Beyond Packed Tower Aeration. In *Florida Water Resources Journal* (Issue July).

Dyksen, J. E. (2012). Aeration and Stripping. In *Water Treatment Plant Design* (p. 98). McGraw-Hill Education. https://www.accessengineeringlibrary.com/content/book/9780071745727/chapter/chapter6

El Azher, N., Gourich, B., Vial, C., Soulami, M. B., & Ziyad, M. (2008). Study of ferrous iron oxidation in Morocco drinking water in an airlift reactor. *Chemical Engineering and Processing*, *47*, 1877–1886. https://doi.org/10.1016/j.cep.2007.10.013

Ford, H. W. (1994). Iron Ocre and related sludge deposits in subsurface drains lines. In *Circular 671 Florida Cooperative*. http://edis.ifas.ufl.edu.

García-Ávila, F., Zhindón-Arévalo, C., Álvarez- Ochoa, R., Donoso-Moscoso, S., Tonon-Ordoñez, M. D., & Flores del Pino, L. (2020). Optimization of water use in a rapid filtration system: A case study. *Water-Energy Nexus*, *3*, 1–10. https://doi.org/10.1016/j.wen.2020.03.005

Gauntlett, R. B. (1980). *A literature review of CO2 removal by aeration* (Issue April). Water Research Centre. https://www.ircwash.org/resources/literature-review-co2-removal-aeration

Gregory, J. (1984). Flocculation and Filtration of Colloidal Particles. In R. F. Davis, H. Palmour, & R. L. Porter (Eds.), *Emergent Process Methods for High-Technology Ceramics* (pp. 59–70). Springer US. https://doi.org/10.1007/978-1-4684-8205-8_4

Hatenboer-Water. (2020). *Effluent Treatment Plant Data*. Hatenboer-Water.

Hem, J. D. (1985). Study and interpretation of the chemical characteristics of natural water. In *US Geological Survey Water-Supply Paper* (Vol. 2254).

Hernandez-Alvarado, F., Kalaga, D. V., Turney, D., Banerjee, S., Joshi, J. B., & Kawaji, M. (2017). Void fraction, bubble size and interfacial area measurements in co-current downflow bubble column reactor with microbubble dispersion. *Chemical Engineering Science*, *168*, 403–413. https://doi.org/10.1016/j.ces.2017.05.006

Hu, R. (2020). *Adsorption of Organic Micro-pollutants by Zeolite Granules: Batch and Column Studies* [Master Thesis TU Delft]. https://repository.tudelft.nl/islandora/object/uuid%3A269fbf06-6714-436c-852f-bd99e0ee7c1a

Huber, P. (2011). Kinetics of CO 2 stripping and its effect on the saturation state of CaCO 3 upon aeration of a CaCO 3-CO 2-H 2O system: Application to scaling in the papermaking process. *Industrial and Engineering Chemistry Research*, *50*(24), 13655–13661. https://doi.org/10.1021/ie200956z

Humbird, D., Davis, R., & Mcmillan, J. D. (2017). Aeration costs in stirred-tank and bubble column bioreactors. *Biochemical Engineering Journal*, *127*, 161–166. https://doi.org/10.1016/j.bej.2017.08.006

Jakobsen, H. A. (2014a). Bubble column reactors. In *Chemical Reactor Modeling* (pp. 883–933). Springer International Publishing. https://doi.org/10.1007/978-3-319-05092-8_8

Jakobsen, H. A. (2014b). Bubble Column Reactors. In *Chemical Reactor Modeling: Multiphase Reactive Flows* (pp. 883–935). Springer International Publishing. https://doi.org/10.1007/978-3-319-05092-8_8

Jasim, A. (2016). *The impact of heat exchanging internals on hydrodynamics of bubble column reactor* [Master Thesis Missouri University of Science and Technology].

https://scholarsmine.mst.edu/masters_theseshttps://scholarsmine.mst.edu/masters_theses/7507

Jobin, R., & Ghosh, M. M. (1972). Effect of Buffer Intensity and Organic Matter on the Oxygenation of Ferrous Iron. In *Journal (American Water Works Association)* (Vol. 64, Issue 9).

Kaegi, R., Voegelin, A., Folini, D., & Hug, S. J. (2010). Effect of phosphate, silicate, and Ca on the morphology, structure and elemental composition of Fe(III)-precipitates formed in aerated Fe(II) and As(III) containing water. *Geochimica et Cosmochimica Acta*, *74*(20), 5798–5816. https://doi.org/10.1016/j.gca.2010.07.017

Kantarci, N., Borak, F., & Ulgen, K. O. (2005). Bubble column reactors. *Process Biochemistry*, *40*(7), 2263–2283. https://doi.org/10.1016/j.procbio.2004.10.004

Kneen, B., Lemley, A., & Wagenet, L. (1995). Reverse Osmosis Treatment of Drinking Water. In *Cornell Cooperative Extension* (Vol. 4). https://doi.org/10.1016/c2013-0-00776-1

Knocke, W. R., Conley, L. A., & Van Benschoten, J. E. (1992). Impact of dissolved organic carbon on the removal of iron during water treatment. In *Water Research* (Vol. 26, Issue 11). https://doi.org/10.1016/0043-1354(92)90072-C

Koweek, D. A., Mucciarone, D. A., & Dunbar, R. B. (2016). Bubble Stripping as a Tool to Reduce High Dissolved CO2 in Coastal Marine Ecosystems. *Environmental Science and Technology*, *50*(7), 3790–3797. https://doi.org/10.1021/acs.est.5b04733

Krishna, R., De Swart, J. W. A., Ellenberger, J., Martina, G. B., & Maretto, C. (1997). Gas Holdup in Slurry Bubble Columns: Effect of Column Diameter and Slurry Concentrations. *AIChE Journal*, *43*(2), 311–316. https://doi.org/10.1002/aic.690430204

Lantec. (2013). *CO2 degasifiers packed with LANPAC cut the cost of drinking water pH adjustment to comply with EPA Lead and Copper Rule.* http://www.lantecp.com

Lerk, C. F. (1965). *Enkele Aspecten van de Ontijzering van Grondwater*. Technische Hogeschool Delft.

Lochrane, T. G. (1977). *Removal of Hydrogen Sulfide from Ground Water in Central Florida* [Master Thesis University of Central Florida]. https://stars.library.ucf.edu/rtd/354

Madaeni, S. S., & Koocheki, S. (2010). Influence of di-hydrogen phosphate ion on performance of polyamide reverse osmosis membrane for nitrate and nitrite removal. *Journal of Porous Materials*, *17*(2), 163–168. https://doi.org/10.1007/s10934-009-9276-5

Marboe, E. C., & Weyl, W. A. (1947). Staining of Glass Containers in Contact With Iron. *Journal of the American Ceramic Society*, *30*(10), 320–322. https://doi.org/10.1111/j.1151-2916.1947.tb18858.x

Mitra, A. K., & Matthews, M. L. (1985). Effects of pH and phosphate on the oxidation iron in aqueous solution. In *International Journal of Pharmaceutics* (Vol. 23).

Molinari, R., Argurio, P., & Romeo, L. (2001). Studies on interactions between membranes (RO and NF) and pollutants (SiO2, NO3-, Mn++ and humic acid) in water. In *Desalination* (Vol. 138, Issues 1–3). https://doi.org/10.1016/S0011-9164(01)00273-9

Murray-Smith, D. J. (2015). Sensitivity Analysis for Model Evaluation. In *Testing and Validation of Computer Simulation Models: Principles, Methods and Applications* (pp. 49–60). Springer International Publishing. https://doi.org/10.1007/978-3-319-15099-4_4

Netafim. (2012). *Recommendations for the Control of Iron in Drip Irrigation Systems*. https://www.netafimusa.com/4ae7ba/contentassets/08b5c208804f4ee8a5003350dae38761/control-of-iron.pdf

Parkhurst, D. L., & Appelo, C. A. J. (1999). *User's Guide to PHREEQC (Version 2) A Computer Program for Speciation, Batch Reaction, One-Dimensional Transport, and Inverse Geochemical*

Calculations (Issue Version 2). U.S. Geological Survey.

Pullin, M. J., & Cabaniss, S. E. (2003). The effects of pH, ionic strength, and iron-fulvic acid interactions on the kinetics of non-photochemical iron transformations. I. Iron(II) oxidation and iron(III) colloid formation. *Geochimica et Cosmochimica Acta*, *67*(21), 4067–4077. https://doi.org/10.1016/S0016-7037(03)00366-1

Raschig. (2020). *Water Degasification-CO2 Removal / Air Stripping Explained*. https://raschig-usa.com/wp-content/uploads/2020/pdf/CO2 Degasifier Design w TM.pdf

Saleh, F. M. A. (1981). *Theory of granular bed filtration and contact flocculation*. 338. http://lib.dr.iastate.edu/rtd/6995/

Santana-Casiano, J. M., Gonzalez-Davila, M., Jesus Rodrıguez, M., & Millero, F. J. (2000). The effect of organic compounds in the oxidation kinetics of Fe II. In *Marine Chemistry* (Vol. 70). www.elsevier.nlrlocatermarchem

Schoeman, J. J., & Steyn, A. (2003). Nitrate removal with reverse osmosis in a rural area in South Africa. In *Desalination* (Vol. 155, Issue 1). https://doi.org/10.1016/S0011-9164(03)00235-2

Senn, A. C., Hug, S. J., Kaegi, R., Hering, J. G., & Voegelin, A. (2018). Arsenate co-precipitation with Fe(II) oxidation products and retention or release during precipitate aging. *Water Research*, *131*, 334–345. https://doi.org/10.1016/j.watres.2017.12.038

Sharma, S. K. (2001). *Adsorptive iron removal from groundwater* [Doctoral Dissertation IHE Delft]. https://research.wur.nl/en/publications/adsorptive-iron-removal-from-groundwater

Sommerfeld, E. O. (1999). Iron and Manganese Removal Handbook. In *American Water Works Association*.

Sposito, G. (2008). *The Chemistry of Soils*. Oxford University Press (OUP). https://books.google.nl/books?hl=en&lr=&id=XCJnDAAAQBAJ&oi=fnd&pg=PR9&ots=iHk9jYxY0A&sig=ylZmPGU98UFKlsNC0DFbSb2iSpE&redir_esc=y#v=onepage&q&f=false

Stumm, W., & Lee, G. F. (1961). Oxygenation of Ferrous Iron. In *Industrial & Engineering Chemistry* (Vol. 53, Issue 2). https://doi.org/10.1021/ie50614a030

Summerfelt, S. T., Davidson, J., & Waldrop, T. (2003). Evaluation of full-scale carbon dioxide stripping columns in a coldwater recirculating system. *Aquacultural Engineering*, *28*(3–4), 155–169. https://doi.org/10.1016/S0144-8609(03)00026-8

Summerfelt, S. T., Zühlke, A., Kolarevic, J., Kristin, B., Reiten, M., Selset, R., Gutierrez, X., & Terjesen, F. (2015). Effects of alkalinity on ammonia removal, carbon dioxide stripping, and system pH in semi-commercial scale water recirculating aquaculture systems operated with moving bed bioreactors. *Aquacultural Engineering*, *65*, 46–54. https://doi.org/10.1016/j.aquaeng.2014.11.002

Sung, W., & Morgan, J. J. (1980). Kinetics and Product of Ferrous Iron Oxygenation in Aqueous Systems. *Environmental Science and Technology*, *14*(5), 561–568. https://doi.org/10.1021/es60165a006

Tamura, H., Goto, K., & Nagayama, M. (1976a). Effect of anions on the oxygenation of ferrous ion in neutral solutions. *Journal of Inorganic and Nuclear Chemistry*, *38*(1), 113–117. https://doi.org/10.1016/0022-1902(76)80061-9

Tamura, H., Goto, K., & Nagayama, M. (1976b). The effect of ferric hydroxide on the oxygenation of ferrous ions in neutral solutions. In *Corrosion Science* (Vol. 16, Issue 4). Pergamon Press. https://doi.org/10.1016/0010-938X(76)90046-9

Tirunehe, G., & Norddahl, B. (2016). The influence of polymeric membrane gas spargers on hydrodynamics and mass transfer in bubble column bioreactors. *Bioprocess and Biosystems*

Engineering, *39*(4), 613–626. https://doi.org/10.1007/s00449-016-1543-7

Tonner, J. B., & Tonner, J. (2004). Desalination and Energy Use. *Encyclopedia of Energy*, 791–799. https://doi.org/10.1016/b0-12-176480-x/00403-4

TU Delft. (2004a). Aeration and Gas stripping. In *Water Treatment*. TU Delft. http://ocw.tudelft.nl/fileadmin/ocw/courses/DrinkingWaterTreatment1/res00071/embedded/!4165726174696f6e20616e6420476173205374726970707 0696e6732303037.pdf

TU Delft. (2004b). Granular Filtration. In *Water Treatment*. TU Delft. https://ocw.tudelft.nl/wp-content/uploads/Granular-filtration-Hydraulics.pdf

Tüfekci, N., & Sarikaya, H. Z. (1996). Catalytic effects of high Fe(III) concentrations on Fe(II) oxidation. *Water Science and Technology*, *34*(7–8), 389–396. https://doi.org/10.2166/wst.1996.0646

Van Beek, C. G. E. M., Dusseldorp, J., Joris, K., Huysman, K., Leijssen, H., Schoonenberg Kegel, F., De Vet, W. W. J. M., Van De Wetering, S., & Hofs, B. (2016). Contributions of homogeneous, heterogeneous and biological iron(II) oxidation in aeration and rapid sand filtration (RSF) in field sites. *Journal of Water Supply: Research and Technology - AQUA*, *65*(3), 195–207. https://doi.org/10.2166/aqua.2015.059

Van Beek, C. G. E. M., Hiemstra, T., Hofs, B., Nederlof, M. M., Van Paassen, J. A. M., & Reijnen, G. K. (2012). Homogeneous, heterogeneous and biological oxidation of iron(II) in rapid sand filtration. *Journal of Water Supply: Research and Technology - AQUA*, *61*(1), 1–13. https://doi.org/10.2166/aqua.2012.033

van Boxel, J. (1998). Numerical model for the fall speed of raindrops in a rainfall simulator. *I.C.E Special Report*, *1998*(1), 77–85. https://dare.uva.nl

van der Helm, A. W. C. (1998). *Modellering van intensieve gasuitwisselingssystemen* [Master Thesis TU Delft]. https://repository.tudelft.nl/islandora/object/uuid%3A1cd73271-6b82-450c-b470-3b817fbbca37

Voegelin, A., Kaegi, R., Frommer, J., Vantelon, D., & Hug, S. J. (2009). Effect of phosphate, silicate, and Ca on Fe(III)-precipitates formed in aerated Fe(II)- and As(III)-containing water studied by X-ray absorption spectroscopy. *Geochimica et Cosmochimica Acta*, *74*, 164–186. https://doi.org/10.1016/j.gca.2009.09.020

Vries, D., Bertelkamp, C., Schoonenberg Kegel, F., Hofs, B., Dusseldorp, J., Bruins, J. H., de Vet, W., & van den Akker, B. (2017). Iron and manganese removal: Recent advances in modelling treatment efficiency by rapid sand filtration. *Water Research*, *109*, 35–45. https://doi.org/10.1016/j.watres.2016.11.032

Wick, K., Heumesser, C., & Schmid, E. (2012). Groundwater nitrate contamination: Factors and indicators. *Journal of Environmental Management*, *111*(3), 178–186. https://doi.org/10.1016/j.jenvman.2012.06.030

Yao, W., & Millero, F. J. (1996). Oxidation of hydrogen sulfide by hydrous Fe(III) oxides in seawater. In *Marine Chemistry* (Vol. 52, Issue 1). https://doi.org/10.1016/0304-4203(95)00072-0

Zhang, H., Zhang, X., Yi, X., He, F., Niu, F., & Hao, P. (2021). Effect of wettability on droplet impact: Spreading and splashing. *Experimental Thermal and Fluid Science*, *124*. https://doi.org/10.1016/j.expthermflusci.2021.110369

Zinati, G., & Shuai, X. (2005). *Management of Iron in Irrigation Water* (No. 516; Fact Sheet). https://njaes.rutgers.edu/fs516/

Appendices

Appendix A. Phreeqc code for Iron oxidation

```
# Definition of mobile iron floc as dissolved species
SOLUTION_MASTER_SPECIES
Iron_floc Iron_floc 0.0 1 1
Fe_two      Fe_two+2    0.0       Fe_two       55.847
Fe_three      Fe_three+3    0.0    Fe_three      55.847

SOLUTION_SPECIES
Iron_floc = Iron_floc
log_k 0.0
Fe_two+2 = Fe_two+2
          log_k   0.0
Fe_two+2 + H2O = Fe_twoOH+ + H+
           log_k   -9.5
          delta_h 13.20   kcal
Fe_two+2 + 2H2O = Fe_two(OH)2 + 2H+
          log_k    -20.494
          delta_h 119.62  kJ
Fe_two+2 + 3H2O = Fe_two(OH)3- + 3H+
          log_k    -28.991
          delta_h 126.43  kJ
Fe_two+2 + H2PO4- = Fe_twoH2PO4+
          -log_k   2.7
          -gamma           5.4       0
Fe_two+2 + HPO4-2 = Fe_twoHPO4
          -log_k   3.6
Fe_three+3 = Fe_three+3
           log_k   0.0
Fe_three+3 + H2O = Fe_threeOH+2 + H+
           log_k   -2.19
           delta_h 10.4   kcal
Fe_three+3 + 2 H2O = Fe_three(OH)2+ + 2 H+
            log_k   -5.67
             delta_h 17.1   kcal
Fe_three+3 + 3 H2O = Fe_three(OH)3 + 3 H+
           log_k   -12.56
          delta_h 24.8   kcal
Fe_three+3 + HPO4-2 = Fe_threeHPO4+
          -log_k   5.43
          -delta_h 5.76     kcal
          -gamma           5.0       0
Fe_three+3 + H2PO4- = Fe_threeH2PO4+2
          -log_k   5.43
          -gamma           5.4       0
```

```
END

PHASES
Goethite
        Fe_threeOOH + 3 H+ = Fe_three+3 + 2 H2O
         log_k   -1
Fe(OH)3(a)
        Fe_three(OH)3 + 3 H+ = Fe_three+3 + 3 H2O
        -log_k   4.891
END

#Defining permeate characteristics
SOLUTION 1
pH     5.9
units mmol/L
temp 10.5
pe 10.0 O2(g) -0.67
N(5)      0.2
Ca        0.2
Na        0.2
K         0.07
Cl        0.1
S         0.07
#P        0.04
Si        0.07
Mn(+2) 0.0007
Fe_two 0.0222              #mmol/L
Fe_three 0
Alkalinity 1 as HCO3
EQUILIBRIUM_PHASES 1
  O2(g)          -0.67

RATES
Fe_two_ox #oxidation of Fe(II)
-start
10  Fe_two = TOT("Fe_two")
20  if (Fe_two <= 0) then goto 200
30  p_o2 = 10^(SI("O2(g)"))
40  moles = (5.4e11 * (ACT("OH-"))^2 * p_o2) * Fe_two * TIME
200 SAVE moles
-end

KINETICS 1
Fe_di_ox
     -formula  Fe_two  -1.0 O2 -0.25 H2O -0.5 Fe_three 1.0 OH- 1.0
     -steps 300 600 900 1200 1500 1800 2100 2400 2700 3000 3300 3600

SELECTED_OUTPUT
```

```
    -file #filename.sel
    -reset false
USER_PUNCH
-headings Minutes  Fe(2)mg/L  Fe(3)mg/L  pH
10 PUNCH SIM_TIME/60 TOT("Fe_di")*55845, TOT("Fe_tri")*55845, -LA("H+")
END
```

Appendix B. Effect of phosphate on iron oxidation and flocculation

Previous studies have shown that phosphate hinders the flocculation of Fe(III)hydroxides (Kaegi et al., 2010; Mitra & Matthews, 1985; Voegelin et al., 2009). However, they did not visualize the speciation of the iron to show the effect of phosphate on the flocculation of Fe(III). Furthermore, no recent studies have investigated the effect of phosphate on Fe(II) oxidation. Voegelin et al. (2009) studied the effect of phosphate on Fe(III) flocculation but did not mention the effect on the oxidation rate of Fe(II).

When 0.04 mmol/L NaH_2PO_4 was added to the solution, the oxidation rate of Fe(II) became slower compared to without $H_2PO_4^-$ at the same pH. With 0.04 mmol/L $H_2PO_4^-$ at pH_{init} of 7, only 22% of the initial Fe(II) concentration was oxidized in 60 minutes compared to 56% in the solution without $H_2PO_4^-$. At pH_{init} of 8, 87% of the Fe(II) was oxidized in 60 minutes in the solution with $H_2PO_4^-$, whereas the Fe(II) was fully oxidized in the solution without $H_2PO_4^-$.

Moreover, the precipitation of Fe(III)hydroxide was also hindered. As can be seen in **Figure A. 1Error! Reference source not found.**, the size of most of the Fe(III) was < 0.2 µm. In contrast, the size of the Fe(III) was >0.2 µm when no phosphate was added as can be seen in **Figure 4. 5**.

The retardation of Fe(III) flocculation happens because phosphate limits Fe(III) polymerization into small Fe(III) monomers and oligomers (Kaegi et al., 2010). Moreover, phosphate-rich Fe(III)-precipitates are negatively charged at near-neutral pH and colloidally more stable than pure Fe(III)hydroxides, preventing them to form bigger flocs (Kaegi et al., 2010; Rose et al., 1996; Tessenow, 1974).

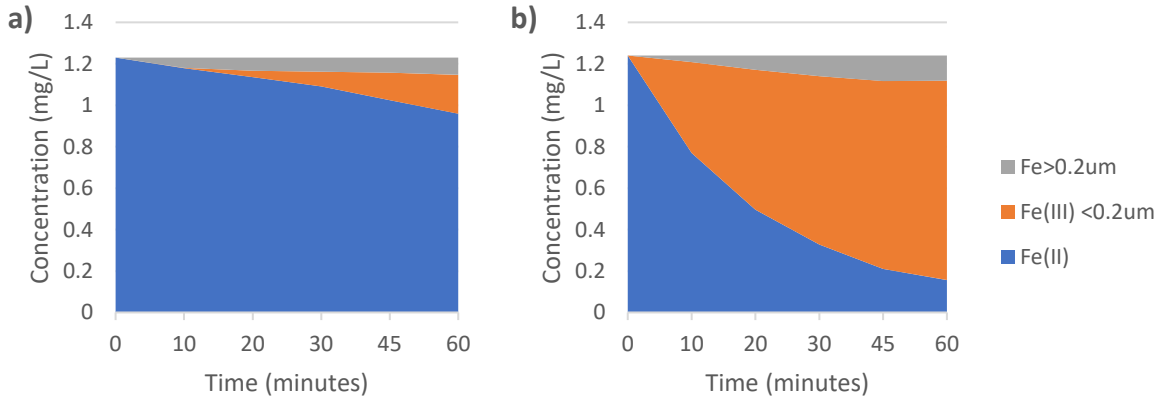

Figure A. 1 Speciation of oxidation products of Fe(II) in the presence of 0.04 mmol/L of $NaH_2PO_4^-$ at a) pH_{init} 7, and b) pH_{init} 8

In contrast to the experiment, simulation using PhreeqC generates a higher oxidation rate for the solution containing phosphate of 0.04 mmol/L, although the difference was not much. Phreeqc automatically speciate the phosphate into $H_2PO_4^-$ and HPO_4^{2-}. The results for PhreeqC Fe(II) oxidation simulation in solutions containing no phosphate and 0.04 mmol/L phosphate is shown in **Table A. 1**.

Table A. 1 Effect of phosphorus on iron oxidation (Phreeqc result)

minutes	Fe(II) (mg/L)		pH	
	P 0	P 0.04 mmol/L	P 0	P 0.04 mmol/L
0	1.239	1.239	8.00	8.00
10	0.239	0.199	7.63	7.67
20	0.095	0.070	7.60	7.64

30	0.042	0.028	7.58	7.63

In both experiment and simulation, the decrease of pH during oxidation did happen as can be seen in **Figure A. 2**. The pH change was greater in the solution without phosphate compared to the one with phosphate. The buffering capacity of phosphate to prevent excessive pH drop during Fe(II) oxidation might be the reason why Phreeqc and some previous studies found a faster oxidation rate in the solution containing $H_2PO_4^-$.

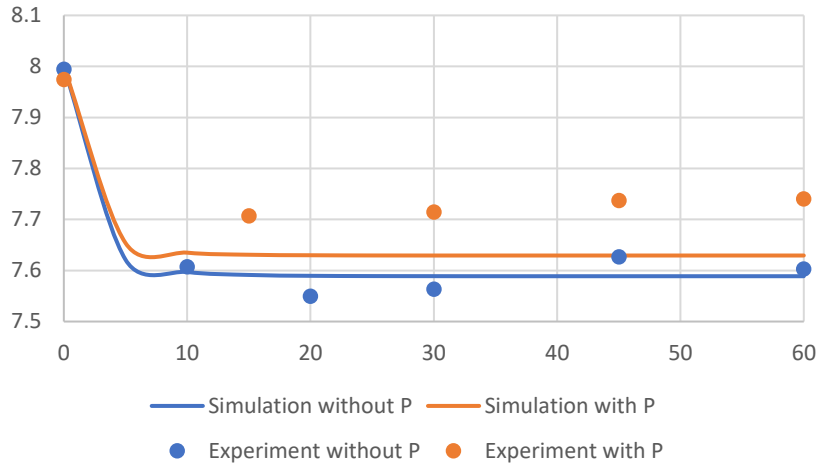

Figure A. 2 Changes of pH during oxidation experiment and simulation in solution without phosphate and containing phosphate

Although the experiment in this study found a slower oxidation rate of Fe(II) in the presence of $H_2PO_4^-$, previous studies found different results. According to Tamura et al. (1976), $H_2PO_4^-$ increases the oxidation rate of Fe(II) into Fe(III), whereas Mitra & Matthews (1985) found that $H_2PO_4^-$ does not affect the reaction. Instead, Mitra and Matthews found that another form of phosphate, HPO_4^{2-} has a catalytic effect on Fe(II) oxidation.

The higher ionic strength with the presence of phosphate could be the cause of the slower oxidation rate. However, the higher pH during the experiment should have made the oxidation faster. Alas, no literature has been found that can explain why the oxidation rate of Fe(II) in this study is slower when phosphate is present

Appendix C. Comparison of adsorption breakthrough between this experiment and Sharma's (2001) finding

The comparison of adsorption breakthroughs is shown in the figure below. The adsorption breakthrough experiment in this study was conducted at pH 6. The breakthrough from this experiment is shown by the red dot, while Sharma's finding is shown in black.

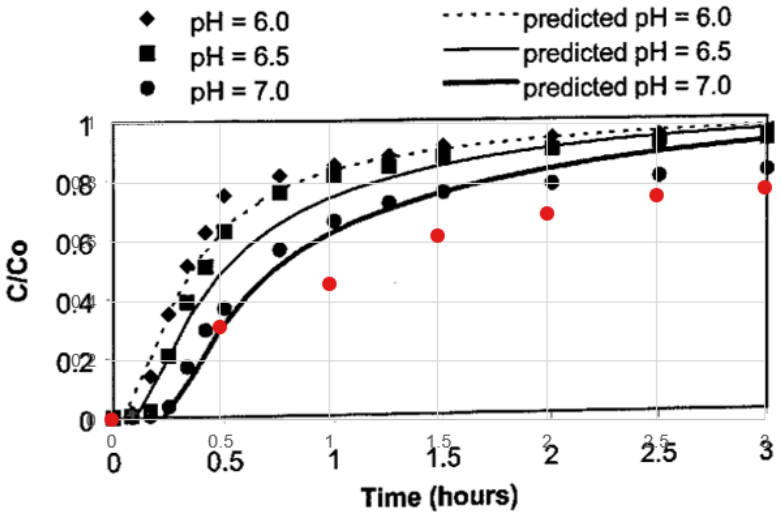

Source: Sharma (2001)

Appendix D. Historical water characteristics of the treatment plant

Parameters	05/03/2020			20/04/2020				13/05/2020				17/06/2020		15/04/2021			
	Before RO	After RO	Inside Aerator	Before RO	After RO	Before SF	After SF	Before RO	After RO	Before SF	After SF	Inside Aerator	After SF	Before RO	After RO	Before SF	After SF
pH	6.9	5.9	6	6.8	3.7	6.4	6.4	7.1	6.2	7	6.8	6.7	6.9	7.7	5.76	6	6.25
EC_mS/cm	0.4	<0.1	<0.1	0.5	0.3	<0.1	<0.1	0.4	<0.1	<0.1	<0.1	<0.1	0.1	0.4	<0.1	<0.1	<0.1
NH4_ppm	<1.9	<1.9	<1.9	<1.9	<1.9	<1.9	<1.9	<1.9	<1.9	<1.9	<1.9	<1.9	<1.9	<1.9	<1.9	<1.9	<1.9
K_ppm	<4	<4	<4	<4	<4	<4	<4	<4	<4	<4	<4	<4	<4	<4	<4	<4	<4
Na_ppm	9.2	4.6	4.6	9.2	14	2.3	2.3	9.2	4.6	2.3	4.6	4.6	4.6	9.2	4.6	4.6	4.6
Ca_ppm	60	8	4	64	24	4	4	64	8	4	4	4	4	60	4	4	4
Mg_ppm	4.9	<2.5	<2.5	4.9	<2.5	<2.5	<2.5	4.9	<2.5	<2.5	<2.5	<2.5	<2.5	4.9	<2.5	<2.5	<2.5
NO3_ppm	149	12	19	19	6.3	6.3	6.3	6.3	6.3	6.3	6.3	6.3	6.3	12	6.2	6.2	12
Cl_ppm	18	3.5	3.6	21	18	3.6	3.6	18	18	3.6	3.6	7.1	3.5	21	3.5	3.5	3.5
S_ppm	<3.3	<3.3	<3.3	<3.3	<3.3	<3.3	<3.3	<3.3	<3.3	<3.3	<3.3	<3.3	<3.3	<3.3	<3.3	<3.3	<3.3
HCO3_ppm	244	67	55	226	37	55	37	189	49	43	31	24	31	220	24	31	31
P_ppm	<1.3	<1.3	<1.3	<1.3	3.4	<1.3	<1.3	<1.3	<1.3	<1.3	<1.3	<1.3	<1.3	<1.3	<1.3	<1.3	<1.3
Fe(II)_ppb	838	1173	1117	12	10443	12	12	12	1731	12	17	106	12	2390	1090	145	0
Mn_ppb	489	38	38	137	66	22	5.5	489	55	5.5	38	38	5.5	467	33	33	11
Zn_ppb	<6.6	<6.6	<6.6	<6.6	26	1569	20	<6.6	<6.6	<6.6	2288	<6.6	<6.6	<6.6	<6.6	<6.6	<6.6
B_ppb	<11	<11	<11	22	36	16	17	17	18	18	21	<11	18	<11	<11	<11	<11
Cu_ppb	<6.4	<6.4	<6.4	<6.4	13	267	<6.4	<6.4	<6.4	<6.4	32	<6.4	<6.4	<6.4	<6.4	<6.4	<6.4
Mo_ppb	<9.6	<9.6	<9.6	<9.6	<9.6	<9.6	29	<9.6	<9.6	<9.6	<9.6	<9.6	<9.6	<9.6	<9.6	<9.6	<9.6
Si_ppm	12	2	2.2	12	5.6	1.7	1.7	12	3.4	1.7	2	2	2	12		2	2
Fe-tot_ppb	22562	1284	1229	670	10611	251	12	18430	1787	11	2066	726	11	6160	1140	210	0

Appendix E. Specification of the tower aerator and rapid sand filtration

Specification of tower aerator

	Value	Unit
Q water	35	m^3/hour
Tower height	3600	mm
Tower diameter	900	mm
Reservoir height	1300	mm
Reservoir diameter	1850	mm

Specification of sand filter

	Value	Unit
Number of sand filter	2	-
Q/column	17	m^3/hour
Bed diameter	1800	mm
Bed height	2600	mm
Filling sand	0.7 – 1.25	mm
Design velocity	10	m/hour

Appendix F. Phreeqc code for CO_2 stripping by bubble column reactor

```
SOLUTION 1 #defining solution
#parameters and values

RATES
CO2_stripping
-start
10 S_coo = mol("CO2")
20 kLa = parm(1)
30 rate = kLa * (S_coo - 2.1e-5)  #2.1e-5 mmol/L= equilibrium concentration of CO2
40 moles = rate * TIME
100 SAVE moles
-end

KINETICS 1
CO2_stripping
-formula C -1
-parameters       2.50E-02 #kLa value (s-1)
-m0       1.0000E+4
-steps 10 20 30 40 50 60 120 180 240 300 360 420 480 520 600
```